Immunity

Rapid Enhancer Remodeling and Transcription Factor Repurposing Enable High Magnitude Gene Induction upon Acute Activation of NK Cells

Graphical Abstract

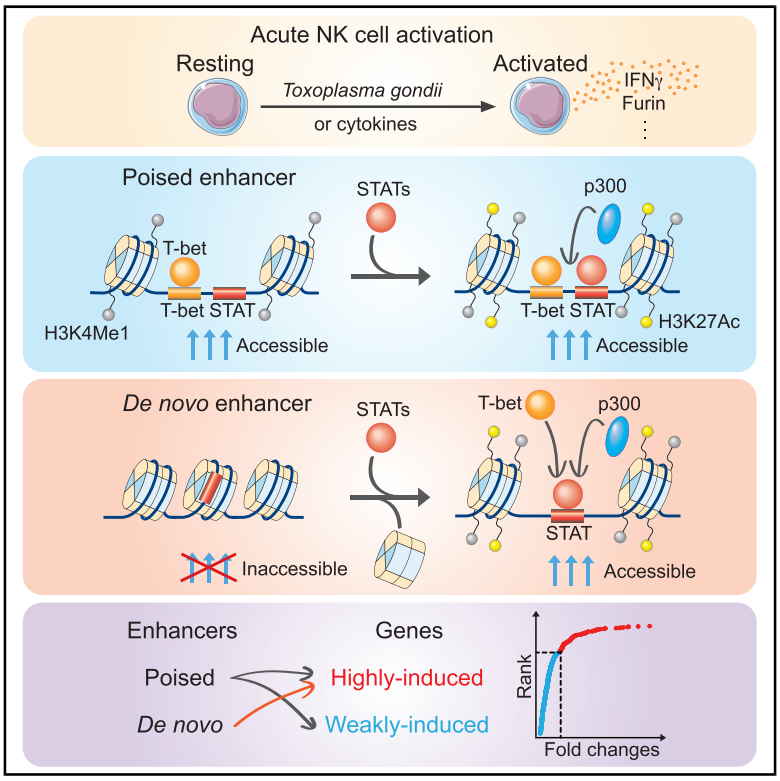

Highlights

- Inducible high-density p300 enhancers form in proximity to highly dynamic genes
- Strong transcriptional induction occurs with both primed and non-primed enhancers
- *De novo* enhancers form *in vivo* during NK cell response to *Toxoplasma gondii* infection
- STATs initiate chromatin opening with T-bet redeployment to non-canonical sites

Authors

Giuseppe Sciumè, Yohei Mikami, Dragana Jankovic, ..., Yuka Kanno, John J. O'Shea, Han-Yu Shih

Correspondence

han-yu.shih@nih.gov

In Brief

During development, innate lymphocytes acquire defined sets of primed enhancers facilitating the rapid immune response. In this issue of *Immunity*, Sciumè et al. delineate the epigenetic changes occurring during acute NK cell activation, revealing the formation of *de novo* enhancers and repurposing of both lineage-determining and signal-regulated transcription factors.

Sciumè et al., 2020, Immunity *53*, 745–758
October 13, 2020 Published by Elsevier Inc.
https://doi.org/10.1016/j.immuni.2020.09.008

Immunity

CellPress

Article

Rapid Enhancer Remodeling and Transcription Factor Repurposing Enable High Magnitude Gene Induction upon Acute Activation of NK Cells

Giuseppe Sciumè,[1,2] Yohei Mikami,[1] Dragana Jankovic,[3] Hiroyuki Nagashima,[1] Alejandro V. Villarino,[1] Tasha Morrison,[1] Chen Yao,[1] Sadie Signorella,[1] Hong-Wei Sun,[4] Stephen R. Brooks,[4] Difeng Fang,[5] Vittorio Sartorelli,[6] Shingo Nakayamada,[1] Kiyoshi Hirahara,[1] Beatrice Zitti,[1] Fred P. Davis,[1] Yuka Kanno,[1,9] John J. O'Shea,[1,9] and Han-Yu Shih[1,7,8,9,10,*]

[1]Lymphocyte Cell Biology Section, Molecular Immunology and Inflammation Branch, National Institute of Arthritis, Musculoskeletal and Skin Diseases, National Institutes of Health, Bethesda, MD 20892, USA

[2]Department of Molecular Medicine, Sapienza University of Rome, Laboratory affiliated to Istituto Pasteur Italia – Fondazione Cenci-Bolognetti, 00185 Rome, Italy

[3]Immunobiology Section, Laboratory of Parasitic Diseases, National Institute of Allergy and Infectious Diseases, National Institutes of Health, Bethesda, MD 20892, USA

[4]Biodata Mining and Discovery Section, National Institute of Arthritis and Musculoskeletal and Skin Diseases, National Institutes of Health, Bethesda, MD 20892, USA

[5]Molecular and Cellular Immunoregulation Section, Laboratory of Immune System Biology, National Institute of Allergy and Infectious Diseases, National Institutes of Health, Bethesda, MD 20892, USA

[6]Laboratory of Muscle Stem Cells and Gene Regulation, National Institute of Arthritis, Musculoskeletal and Skin Diseases, National Institutes of Health, Bethesda, MD 20892, USA

[7]Neuro-Immune Regulome Unit, National Eye Institute, National Institutes of Health, Bethesda, MD 20892, USA

[8]National Institute of Neurological Disorders and Stroke, National Institutes of Health, Bethesda, MD 20892, USA

[9]Senior Author

[10]Lead Contact

*Correspondence: han-yu.shih@nih.gov

https://doi.org/10.1016/j.immuni.2020.09.008

SUMMARY

Innate immune responses rely on rapid and precise gene regulation mediated by accessibility of regulatory regions to transcription factors (TFs). In natural killer (NK) cells and other innate lymphoid cells, competent enhancers are primed during lineage acquisition, and formation of *de novo* enhancers characterizes the acquisition of innate memory in activated NK cells and macrophages. Here, we investigated how primed and *de novo* enhancers coordinate to facilitate high-magnitude gene induction during acute activation. Epigenomic and transcriptomic analyses of regions near highly induced genes (HIGs) in NK cells both *in vitro* and in a model of *Toxoplasma gondii* infection revealed *de novo* chromatin accessibility and enhancer remodeling controlled by signal-regulated TFs STATs. Acute NK cell activation redeployed the lineage-determining TF T-bet to *de novo* enhancers, independent of DNA-sequence-specific motif recognition. Thus, acute stimulation reshapes enhancer function through the combinatorial usage and repurposing of both lineage-determining and signal-regulated TFs to ensure an effective response.

INTRODUCTION

Rapid responses are a hallmark of how metazoan immune and inflammatory systems coordinate the regulation of hundreds of genes, promoting host defense, tissue repair, and metabolism (Phan et al., 2017; Pope and Medzhitov, 2018; Smale and Natoli, 2014; Tong et al., 2016). Innate lymphoid cells (ILCs) play key roles in host defense, especially at epithelial barrier surfaces (Diefenbach et al., 2014; Vivier et al., 2018), functionally mirroring adaptive lymphocyte counterparts (Shih et al., 2014; Spits et al., 2013). A cardinal feature of ILCs is the ability to rapidly respond to environmental challenges, with their transcriptomic programs being primed for rapid induction (Bezman et al., 2012; Robinette et al., 2015). One mechanism that underlies this primed function is the preexisting promoter histone acetylation state of key effector genes (Stetson et al., 2003; Tato et al., 2004). In addition, profiling genome-wide chromatin accessibility of ILCs has revealed that non-coding regulatory regions in proximity to effector genes are selectively exposed and made available to transcription factor (TF) recognition during development, prior to acute activation (Collins et al., 2019; Gury-BenAri et al., 2016; Koues et al., 2016; Lau et al., 2018; Sciumè et al., 2017; Shih et al.,

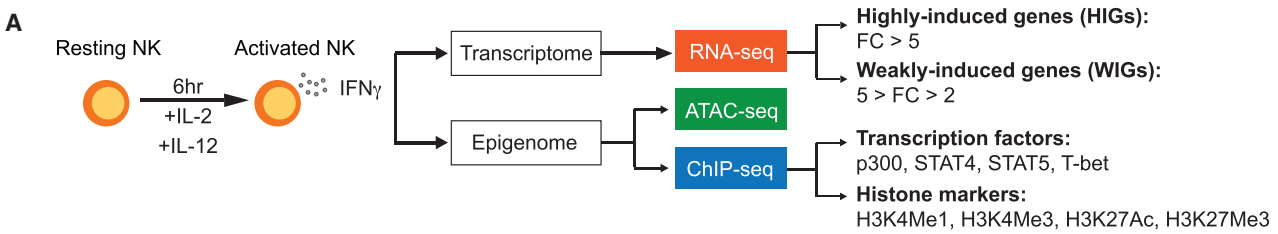

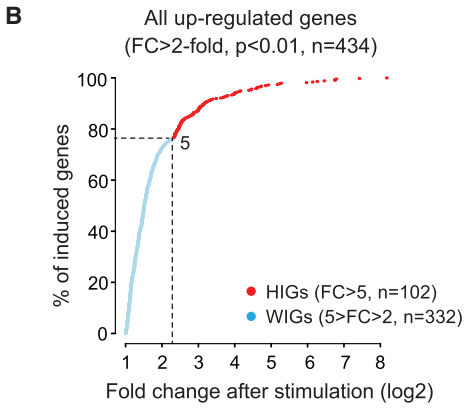

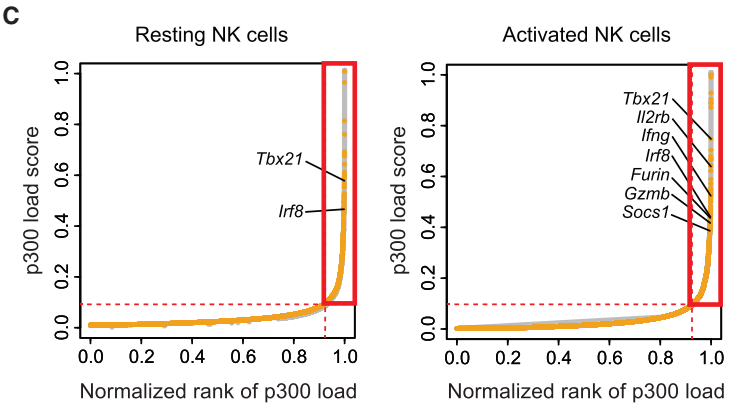

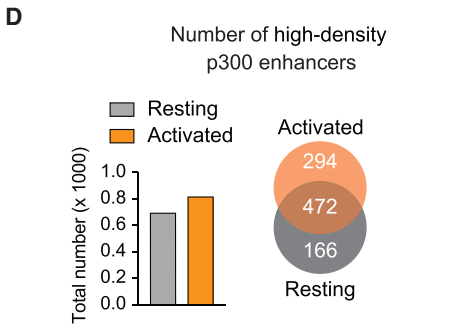

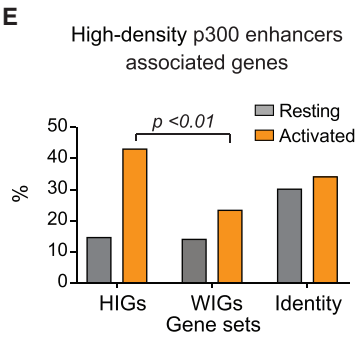

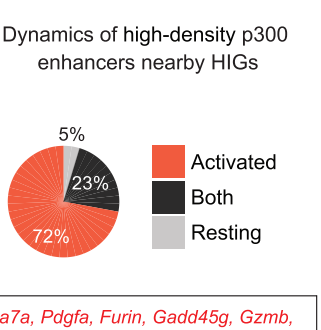

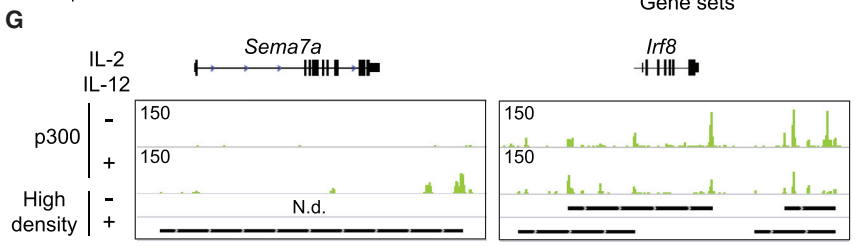

Sema7a, Pdgfa, Furin, Gadd45g, Gzmb, Lss, Il2ra, Casp3, Slc16a6, Cxcr6, Tgfb1, Il6st, Flot1, Sub1, F2rl2, Thy1, Gpr155, Tnks1bp1, Gpr171, Usp18, Nek6, Pim2, Mafg, Ppp1r3b, Ifitm1, Tmem2, Ifng, Hic1, Rbpj, Cish, Ccr5

Xcl1, Nfil3, Maff, Bcl3, Nabp1, Socs1, Irf8, Abcb9, Litaf, Sult2b1

Tnfrsf9, Fosl2

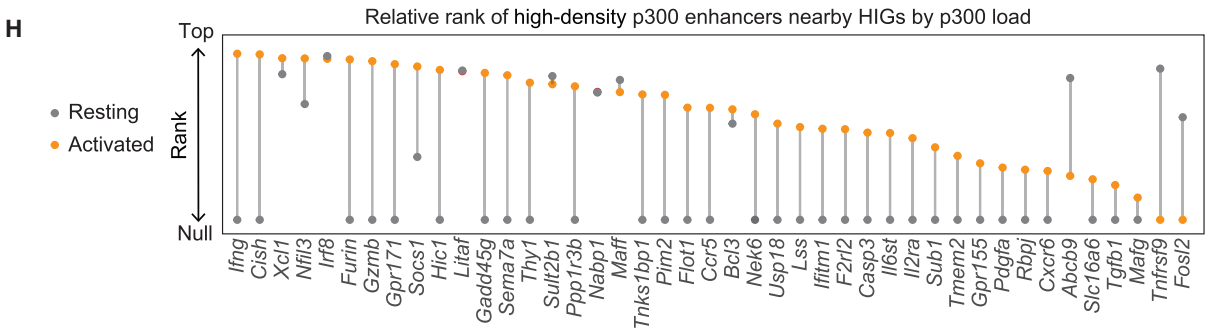

(legend on next page)

2016). The paradigmatic view is that lineage-defining TFs (LDTFs) serve as pioneer factors, responsible for developmental acquisition of chromatin accessibility and "supervising" cell-specific epigenomic status (Heinz and Glass, 2012; Zaret and Carroll, 2011). In contrast, signal-regulated TFs (SRTFs) rapidly alter active enhancer landscapes in response to acute signaling at genomic regions made accessible by LDTFs during development (Bonelli et al., 2014; Glass and Natoli, 2016). During macrophage activation, SRTFs are capable of opening previously packed chromatin regions, generating *de novo* or latent enhancers via LDTFs binding to their cognate sequence-specific motifs (Glass and Natoli, 2016; Kaikkonen et al., 2013; Ostuni et al., 2013). In $CD4^+$ helper T cells, SRTFs are dominant in defining the enhancer repertoires during formation of effector cells in a process that takes several days to occur (Vahedi et al., 2012). Changes of enhancer repertoires have been observed in natural killer (NK) cells acquiring adaptive features during mouse cytomegalovirus (MCMV) infection (Lau et al., 2018). However, these studies reflect longer-term stimulations; given that acute activation is a rapid event, whether epigenetic regulation contributes during such a short period is not clear, nor is the contribution of SRTFs and LDTFs to this process.

The limitations of identifying common features of co-regulated genes require a customized analysis of key genes individually (Tong et al., 2016). Compounding this issue is the recognition of the asymmetric organization of enhancers and extensive modification of selected genomic regions, engaging large amounts of TFs to multiple neighboring enhancer sites that assemble as so-called super- or stretch-enhancers (Hnisz et al., 2013; Lovén et al., 2013; Whyte et al., 2013). In lymphocytes, key effector loci such as cytokine and cytokine receptor genes are enriched for this complex enhancer architecture (Vahedi et al., 2015; Witte et al., 2015). However, a full picture of how different classes of TFs precisely control acute, dynamic chromatin accessibility and enhancer activation and how these events relate to gene expression levels is lacking (Furlong and Levine, 2018; Garber et al., 2012; Hnisz et al., 2016; Smale et al., 2014; Winter and Amit, 2014).

In this study, we set out to address the impact of *in vitro* and *in vivo* acute activation on chromatin remodeling of effector gene loci in NK cells. More specifically, we sought to determine the relationship between the dynamics of enhancer modifications and the magnitude of gene induction. Although preexisting chromatin accessibility was a hallmark of NK cell effector loci, we observed that such a feature was not a prerequisite for all induced genes. In fact, rapid appearance of *de novo* accessibility and activation of complex enhancer landscapes were also involved in high-level transcriptional induction of a large proportion of effector genes driven by SRTFs. We also found the LDTF T-bet was redeployed and repurposed to regions bound by STATs (signal transducers and activators of transcription) in activated NK cells, similar to macrophage LDTF PU.1 upon stimulation (Kaikkonen et al., 2013; Ostuni et al., 2013). Surprisingly though, in contrast to previously proposed recruitment of LDTFs to their cognate DNA motifs, we found that STATs drive the T-bet redeposition to non-canonical DNA-binding sites that lack T-bet motifs. Collectively, our data reveal divergent modes of gene regulation that involve both poised and *de novo* enhancers and alterations in chromatin accessibility in conjunction with a switch in roles between LDTFs and SRTFs as "pioneer factors." In aggregate, this leads to rapid and high-magnitude transcriptomic responses.

RESULTS

Highly Induced Genes (HIGs) Are Linked with Rapid Formation of Complex Active Enhancer Architecture

To define the molecular mechanisms underlying rapid activation in innate lymphocytes, we employed NK cells as a model. Using the well-recognized factors interleukin-12 (IL-12) and IL-2, known as potent inducers of NK cell activation (Marçais et al., 2013), we profiled changes in global transcriptomes and epigenomes after 6 h of cytokine treatment (Figure 1A). An important

Figure 1. Rapid High-Density p300 Enhancer Landscape Formation Is Associated with the Magnitude of Gene Induction

(A) Schematic representation of experimental design. Murine splenic NK cells were stimulated with IL-2 (1,000 U/mL) and IL-12 (10 ng/mL) for 6 h prior to transcriptomic and epigenomic analysis. Transcriptomes of resting and activated NK cells were evaluated using RNA-seq; epigenomes were evaluated by ATAC-seq for chromatin accessibility and ChIP-seq for TF binding and histone mark distribution.

(B) RNA-seq analysis of gene inducibility upon NK cell activation (resting NK, n = 4; activated NK, n = 2; cutoff = 10 FPKM). Fold changes (FCs) of gene induction after 6-h cytokine stimulation (FC > 2; p value < 0.01) were plotted by a cumulative distribution curve. Among 434 upregulated genes, 102 genes were induced more than 5-fold and named HIGs (shown in red), and 332 genes were induced between 2- and 5-fold and named WIGs (shown in blue). The dashed line represents the 5-fold induction threshold. For the FCs and p values of HIGs and WIGs, see Table S1. Statistical significance was assessed with non-paired two-tailed Student's t test. FPKM, fragments per kilobase exon per million mapped reads.

(C) Ranked order of p300-loaded regulatory elements in resting (left) and activated (right) NK cells. High-density p300 enhancers and their scores were determined by proceeding p300 ChIP-seq data using HOMER and were plotted by R. Data are representative of two independent experiments. Rectangles circle the genomic regions characterized as high-density p300 enhancers. For reproducibility between biological replicates, see Figures S1C and S1D. For the intensity of peak signals, see Table S2.

(D) Dynamics of high-density p300 enhancers upon NK activation. Bar graph shows the total number of high-density p300 enhancers in resting and activated NK cells as analyzed in (C). Venn diagram indicates the numbers of unique and shared high-density p300 enhancers between two conditions.

(E) Relationships between dynamic high-density p300 enhancers and the gene sets defined in (B) (HIGs and WIGs) and the ImmGen Project for NK identity genes (Bezman et al., 2012). Bar graph depicts the frequency of genes that are associated with high-density p300 enhancers in resting and activated NK cells for three gene sets. Statistical significance was determined using Fisher's exact test.

(F–H) Dynamics of high-density p300 enhancers nearby HIGs. (F) Percentage of HIGs nearby high-density p300 enhancers that were presented in resting or activated NK cells or both. A list of these genes is shown in the box. (G) Genomic snapshots for *Sema7a* and *Irf8* loci showing p300 binding and presence of high-density enhancers in resting and activated NK cells. N.d., non-detectable. (H) Relative rank of high-density p300 enhancers for HIGs in activated (orange dots) and resting NK cells (gray dots). The highest rank equals to 1. Genes not associated with high-density p300 enhancers were assigned with a pseudo-rank number of 800 as null (most of gray dots).

See also Figure S1 and Tables S1 and S2.

aspect of immune responses is that not only are many genes induced, but also their range of transcriptional activation encompasses multiple orders of magnitude (Tong et al., 2016). The argument has been made therefore that all induced genes may not conform to the same regulatory rules and that HIGs should be considered separately. Among the 434 inducible genes in activated NK cells, we observed a limited set of HIGs (n = 102, genes with at least 5-fold induction) that included several canonical NK cell response genes, such as *Ifng* and *Gzmb*, and TFs, such as *Zbtb32* and *Nfil3* (Figure 1B; Table S1). We identified more weakly induced genes (WIGs; n = 332, genes with 2- to 5-fold induction), including NK cell effector molecules (*Prf1*, encoding perforin), TFs (*Runx1* and *Runx3*), and signal transduction adaptors (*Myd88*). As a class, WIGs were expressed at higher levels prior to stimulation than HIGs, but this difference disappeared after stimulation (Figure S1A). Of note, expression levels of genes underlying NK cell identity, as defined by the Immunological Genome Project (Bezman et al., 2012), remained globally unchanged (Figure S1B).

We have previously demarcated the complex enhancer architecture that encompasses genes defining $CD4^+$ T lymphocyte cell identity, including many effector molecules and key TFs, by measuring the density of deposition of an enhancer marker, histone acetyltransferase p300 (Vahedi et al., 2015). To evaluate the relationship between enhancer-associated complexes and rapid gene induction during innate response, we next cataloged high-density p300 sites in resting and activated NK cells using an algorithm developed for identifying genomic regulatory loci previously designated super-enhancer complexes (Figures 1C, S1C, and S1D; Table S2) (Whyte et al., 2013). Despite comparable numbers of high-density p300-bound regions in resting and activated cells, nearly 40% of these sites were newly acquired after stimulation, indicating a dramatic remodeling of the chromatin landscapes upon NK cell activation (Figure 1D). We next sought to assess the relationship between high-density p300 deposition and the magnitude of gene induction by assigning these regions to the nearest gene. In the resting state, p300-enriched regions were more likely to be associated with NK cell identity genes (~30%) compared to inducible genes (~15% in WIGs and HIGs) (Figure 1E) or other ILC identity genes (<5%) (Figure S1E). While high-level p300 binding in proximity to cell identity genes was largely unaffected by activation, the association of such high-density p300-bound regions with HIGs (>40%) was greater than that of WIGs (~25%) (Figure 1E). Specifically, only a minority of HIG-associated high-density p300 sites, like *Irf8*, were present in resting NK cells (23%), whereas the majority (72%) of HIG-associated p300 enriched loci were further induced following stimulation, as exemplified by *Sema7a* (Figures 1F–1H). This supports the argument made by Smale and colleagues that the regulation of any given gene may be *sui generis* (Tong et al., 2016). The redistribution of p300 load during NK cell activation also involved the loss of 26% of high-density p300 sites present in resting NK cells (Figure 1D), including those near genes that reduce gene expression upon NK cell activation (e.g., *Nr4a1*, *Cxcr4*, and *S1pr5*; Figure S1F).

Our data therefore establish that despite the primed nature of chromatin architecture in NK cells, rapid reprogramming of their transcriptomes upon stimulation involves extensive genome-wide enhancer modifications, including dramatic remodeling of complex enhancer landscapes.

Inducible High-Density p300 Enhancers Exploit Not Only Primed but Also Non-primed Regulatory Regions

The genomic loci encoding critical ILC effector molecules are primed during cellular development, prior to pathogen encounter (Shih et al., 2016). We hypothesized that inducible p300 recruitment might also be preferentially built upon primed regions with preexisting chromatin accessibility. To test this hypothesis, we analyzed the chromatin accessibility (assay for transposase accessible chromatin using sequencing [ATAC-seq]) of regions that rapidly alter their p300 deposition in activated NK cells (Figure S2A). By merging p300 ChIP-seq and ATAC-seq datasets, we defined six major classes of regulatory elements that revealed dynamic epigenetic landscapes (Figure S2A). Although p300 binding is often linked to enhancer activities, we found that in some cases it also binds to promoters (Figure S2B), especially in class 4 regulatory elements, which are enriched for an active promoter mark, H3K4me3 (data not shown). These promoters are more likely to recruit general TFs to maintain chromatin accessibility without the need of active p300 binding. However, to focus on the potential contributions of distal enhancers in gene regulation, we excluded regulatory elements within 1 kb of transcription start sites (TSSs) (Figure 2A; Table S3).

Consistent with our previous findings (Figure S2A), a large portion of new p300-bound sites (49%) were accessible prior to stimulation (Figures 2A, upper right panel, and S2C) and thus are designated "primed" or "poised" enhancers (class 3) (Shih et al., 2016; Stetson et al., 2003). Interestingly though, nearly half of the sites with inducible p300 binding resided in regions that were previously inaccessible in resting NK cells (classes 1 and 2). Among these regions, over half acquired accessibility after activation (class 2, exemplified by gene *Bcl2l10* in Figure 2B), consistent with "latent" or "*de novo*" enhancers described previously in activated macrophages (Kaikkonen et al., 2013; Ostuni et al., 2013). The other half remained inaccessible (class 1) presumably due to inadequate time for chromatin remodeling to occur following p300 recruitment, and thus, we designated these regions as "evolving" enhancers.

Acute activation also resulted in loss of p300 binding in a subset of enhancers (classes 4–6), presumably reflecting the remodeling of previously active enhancers (Figure 2A, bottom right panel, and Figure 2B). We found that most regulatory elements that lost p300 binding remained accessible (54%, class 4), consistent with the notion that p300 binding can be rapidly and dynamically regulated at accessible genomic regions and potentially replaced by other factors that mediate accessibility. In addition, we observed genomic regions that lost both p300 binding and accessibility (31%, class 5), as well as regions that lost p300 binding and remained inaccessible (15%, class 6).

We next explored the activities of these six enhancer classes by evaluating histone modifications, including histone H3 lysine 4 mono-methylation (H3K4me1), marking both active and primed/poised enhancers; histone H3 lysine 27 acetylation (H3K27ac), marking active enhancers; histone H3 lysine 4 tri-methylation (H3K4me3), marking active promoters; and histone H3 lysine 27 tri-methylation (H3K27me3), marking Polycomb-

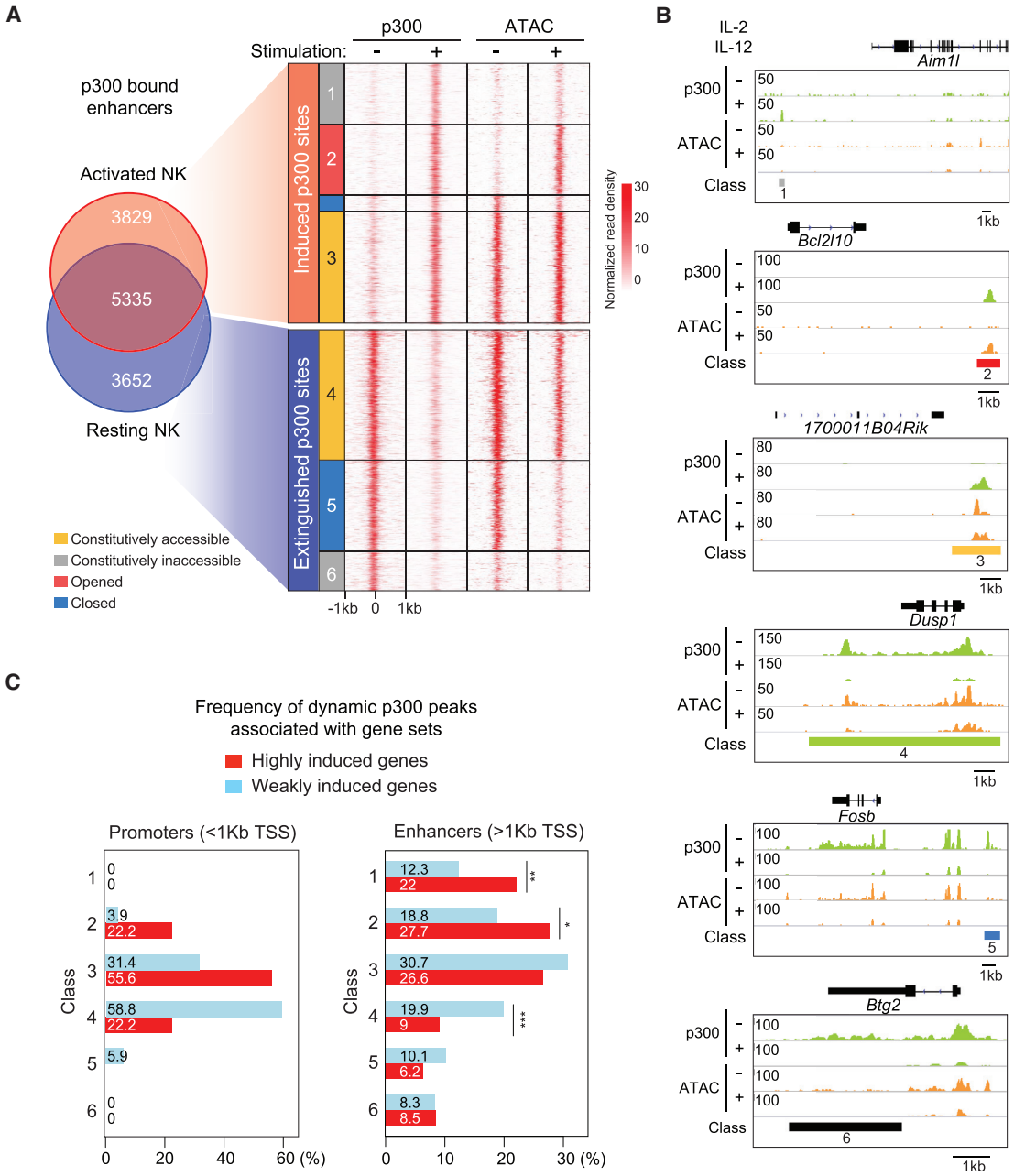

Figure 2. Dynamic Chromatin Landscapes and Their Relationship with Gene Induction upon NK Cell Activation

(A) Venn diagram on the left showing the numbers of status-specific and shared peaks from p300 ChIP-seq replicates (resting NK, n = 2; activated NK, n = 2). The enhancers were defined by p300 binding sites over 1kb distant from TSSs. Peak density heatmap on the right showing p300 load (ChIP-seq) and chromatin accessibility (ATAC-seq) across ±1-kb genomic regions of induced (top) and extinguished (bottom) p300 peaks upon cytokine stimulation. Each row corresponds to a single enhancer region. Combinatorial peak distribution patterns among four mapping results distinguished six major enhancer types (classes 1–6). The normalized read density was determined by HOMER using 10 bp as the bin size. Annotation of nearby genes for each enhancer class is shown in Table S3.

(B) Genomic snapshots depicting p300 load and chromatin accessibility (ATAC-seq) in resting and activated NK cells for representative loci of six major enhancer classes defined in Figure 2A.

(C) Bar graph showing frequency of HIGs (red) and WIGs (blue) associated with each promoter and enhancer class defined by p300 load and chromatin accessibility in Figures 2A and S2A. The enhancers were defined by p300 binding sites over 1 kb distant from TSSs and the promoters were defined as the genomic regions within 1 kb of TSSs. Statistical significance was determined by using Fisher's exact test (*p value < 0.05, **p value < 0.01, and ***p value < 0.001). See also Figures S2 and S3 and Table S3.

repressed regions. H3K27ac levels increased in all three classes of inducible p300-bound sites (classes 1–3) regardless of their chromatin accessibility (Figures S2D and S2E). The higher basal levels of H3K4me1 at class 3 enhancers were consistent with their designation as primed enhancers; however, class 1 and 2 regions acquired modest levels of this modification. Promoter (H3K4me3) and repressive marks (H3K27me3) showed negligible enrichment or changes at inducible enhancer regions. Regions that extinguished p300 binding (classes 4–6), however, remained enriched for both enhancer marks H3K4me1 and H3K27ac (Figures S2D–S2F).

To assess the dynamics of induced changes in the enhancer landscapes upon NK activation, we measured the chromatin accessibility in NK cells over time after stimulation with cytokines (Figures S3A and S3B). We found the accessibility of *de novo* enhancers (class 2) can be detected at 180 min, but not at earlier time points, similar to findings in bone-marrow-derived macrophages (Kaikkonen et al., 2013; Ostuni et al., 2013). Evolving enhancers (class 1) also revealed low levels of chromatin accessibility at 180 min. As discussed below, we observed acquisition of chromatin accessibility of these regions in activated NK cells at 3 days after infection with *Toxoplasma gondii*.

Finally, we sought to evaluate the relationship between the magnitude of rapid gene induction and changes in p300 binding and chromatin accessibility. We first focused on the relationship between p300 deposition on promoters (<1 kb from TSSs) and levels of gene induction. We found that ~60% HIGs were associated with inducible p300 binding in the context of preexisting accessibility (class 3 regulatory regions, Figure 2C, left panel) In contrast, nearly all WIGs were characterized by preexisting accessibility, with the majority being associated with loss of p300 binding (class 4 regions) and a portion being associated with increased p300 binding (class 3).

We anticipated that HIGs would preferentially utilize deposition of p300 on primed enhancer regions, as they were enriched for primed promoters. However, we found that these genes were more likely to be associated with genomic regions with both primed (class 3) and non-primed (classes 1 and 2) enhancers than WIGs (>1 kb from TSSs, Figure 2C, right panel). In contrast, most WIGs were associated with accessible regulatory elements (classes 2–4); although, a portion were associated with inducible accessibility and p300 deposition. Together, our results argue that HIGs and WIGs are regulated in distinct manners; HIGs employ both primed and non-primed regions that contribute to the formation of new high-density enhancer complexes. We concluded that complex enhancer landscapes are highly dynamic during cell activation and positively correlate with the magnitude of gene induction.

NK Cell Activation *In Vivo* Involves Decompaction of Non-primed Enhancers

To assess the relevance of our *in vitro* observations, we next asked whether *in vivo* NK cell activation also requires remodeling of non-primed enhancers. Thus, we assessed transcriptomic and epigenomic changes in NK cells upon *T. gondii* infection, a canonical inducer of a strong IL-12-dependent type 1 immune response (Sher et al., 2003). We analyzed NK cells isolated from spleens and peritoneal exudates on days 3 and 7 after infection, which represent the peak of NK cell and Th1 cell responses in this model, respectively (Goldszmid et al., 2012) (see Figure 3A for the experimental design). Using single-cell RNA sequencing (scRNA-seq), we found that NK cells could be subgrouped into clusters based on their activation and proliferation state (Figures 3B and S4A). For instance, the NK effector genes *Ifng* and *Gzmb* were expressed highest in clusters 2 and 0, respectively, which represents peritoneal cells collected at different time points (Figure S4B). The proliferation marker *Mki67*, on the other hand, was elevated in clusters 6 and 7, which, as expected, mainly comprise NK cells from infected mice (Figure S4B).

We next asked whether genes induced by cytokine stimulation were also activated during *T. gondii* infection. We first defined a module of genes induced by *in vitro* IL-2 and IL-12 co-stimulation. Scoring the transcriptomes of single cells, we found that the IL-2/IL-12 module was enhanced in NK cells at day 3 of infection (especially in peritoneal cells) and declined at day 7 (Figure 3C). In parallel, we asked whether the genes marking the single-cell cluster of "early" activated peritoneal NK cells (cluster 2) were responsive to *in vitro* cytokine stimulation. Indeed, most cluster 2 signature genes were also induced by co-stimulation with IL-12 and IL-2 (Figure S4C).

Having identified transcriptional similarities between NK cells activated *in vitro* and in the early phase of *T. gondii* infection, we next asked how *de novo* enhancer landscapes identified *in vitro* might relate to regulatory regions identified *in vivo* during acute infection. To this end, we profiled chromatin accessibility of NK cells at three time points during *T. gondii* infection (days 0, 3, and 7) and showed that the top two genes marking early activated peritoneal NK cells (single-cell cluster 2), *Furin* and *AA467197*, had newly acquired accessibility (Figure 3D). At a genome-wide level, most of the *de novo* enhancers we identified from *in vitro* activated NK cells (Figure 2A) exhibited acquired accessibility upon *T. gondii* infection (Figures 3E and 3F). Moreover, a portion of the "evolving enhancers" (class 1), p300-bound but inaccessible after 6 h of *in vitro* cytokine stimulation (Figure 2B), became accessible in NK cells upon *T. gondii* infection, indicating that these regions were dynamically regulated and sensitive to the length of stimulation. Together, our data reveal that formation of *de novo* active enhancers is a general epigenomic mechanism that occurs both *in vitro* and *in vivo*.

Genomic Sequence Motifs Define Distinct Classes of Enhancers

To begin dissecting potential molecular mechanisms underlying activation-dependent chromatin remodeling in NK cells, we analyzed the enrichment of consensus TF motifs among the six major classes of regulatory elements defined in Figure 2A. T-bet (encoded by *Tbx21*), ETS, IRF and Runx family TFs were enriched in p300-bound regions that were constitutively accessible in NK cells and did not change with activation (class 3, Figure 4). This finding suggests that these key TFs, contributing to NK cell development (Townsend et al., 2004; Zhang et al., 2018; Ebihara et al., 2015; Rapp et al., 2017; Barton et al., 1998; Choi et al., 2011; Lacorazza et al., 2002), likely shape NK cell chromatin organization during differentiation and specification prior to activation. Motifs for T-bet, (erythroblast transformation specific) ETS, (interferon regulatory factor) IRF, and (runt-

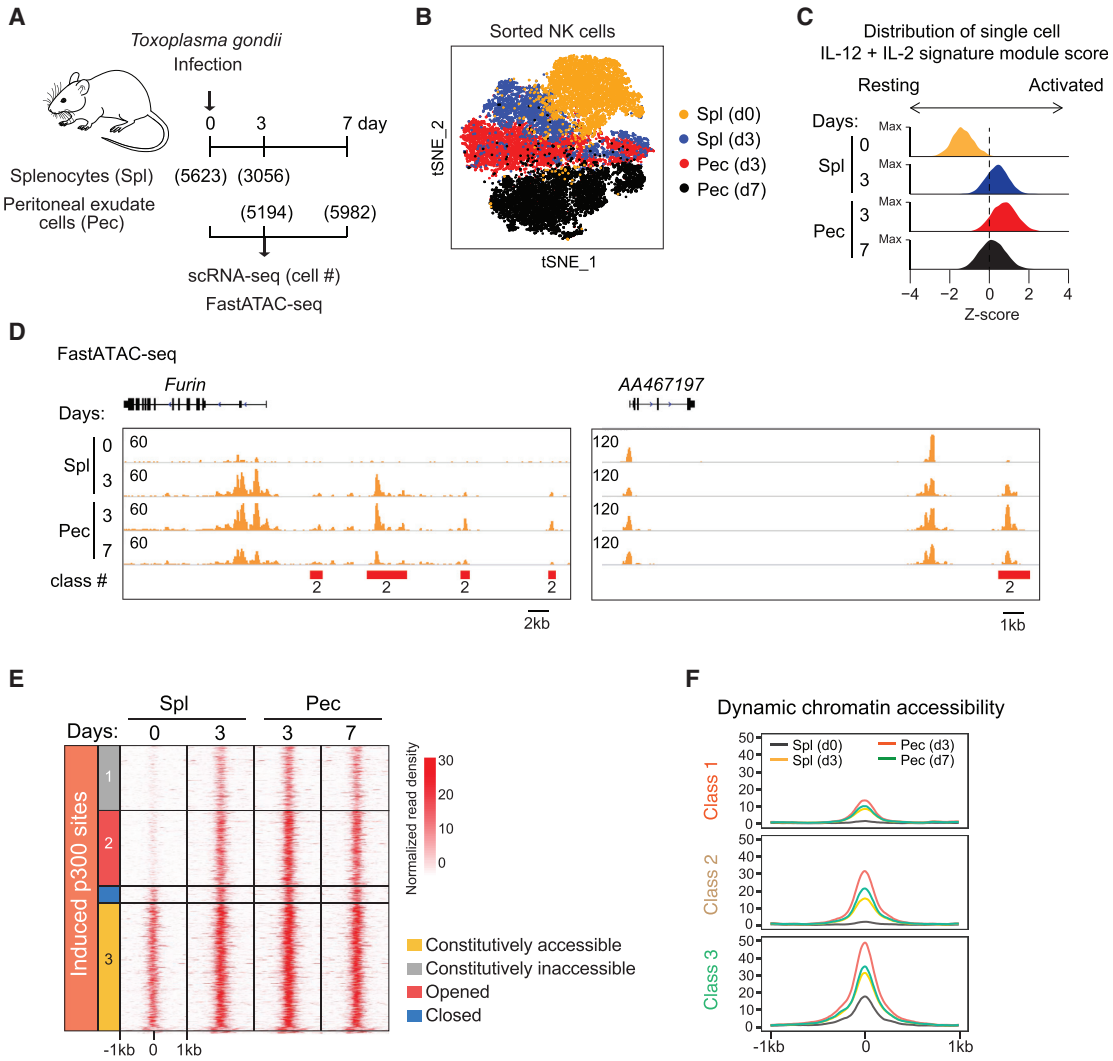

Figure 3. Type 1 Inflammatory Gene Signature and *De Novo* Enhancers Were Formed Early during *Toxoplasma gondii* Infection

(A) Schematic illustration of experimental design. NK cells were sorted from peritoneal cavity exudates (Pec) and spleens (Spl) from *T. -gondii*-infected mice as CD3ε$^-$NKp46$^+$CD49b$^+$ cells. scRNA-seq and FastATAC-seq were performed on splenic (days 0 and 3) and peritoneal (days 3 and 7) NK cells. Captured cell number for each scRNA-seq sample is shown in parenthesis.

(B) The t-distributed stochastic neighbor embedding (t-SNE) plot of scRNA-seq data projecting four sources of NK cells collected as described in (A).

(C) The stacked histogram plot depicting the score of activated NK signature genes in single-cell data obtained after *T. gondii* infection. NK activation signature genes were inferred from bulk mRNA-seq data (Figure 1B). For details of data processing, see STAR Methods.

(D) Representative examples of FastATAC-seq analysis for early inducible HIG loci, *Furin* and *AA467197*, in NK cells upon *T. gondii* infection.

(E) Peak density heatmap of FastATAC-seq peaks in NK cells upon *T. gondii* infection. Peaks were organized based on the classification of induced p300 sites, and their chromatin accessibility shown in Figure 2A.

(F) Histogram plot depicting average distribution of p300 load around the center of induced p300 peaks (±1 kb) of enhancer classes 1–3 in (E). NK cells isolated from Pec after 3 days of *T. gondii* infection (red line) shows highest chromatin accessibility in all three classes. In contrast, non-infected NK cells (d0, black line) revealed minimal chromatin accessibility in classes 1 and 2.

Data are representative of two independent experiments.

See also Figure S4.

related transcription factor) Runx family TFs were also enriched in class 4 regulatory elements that also encompass promoters.

By contrast, we found that motifs from the STAT family were enriched among all regions with inducible p300 binding (classes 1–3), compared to regions that lost p300 binding (classes 4–6; Figure 4). Motifs associated with AP-1 (basic leucine zipper [bZIP]) family members (Bach1, Bach2, Fosl2, Jun, and MafK) paralleled the enrichment pattern of STAT motifs, suggesting that these SRTFs can alter p300 binding profiles by conveying this factor to targets with cognate DNA motifs.

Taken together, our data support the contention that external signals rapidly reorganized active enhancer landscapes by inducing STAT and AP-1-family-driven TF networks. This reorganization involves not only interplay

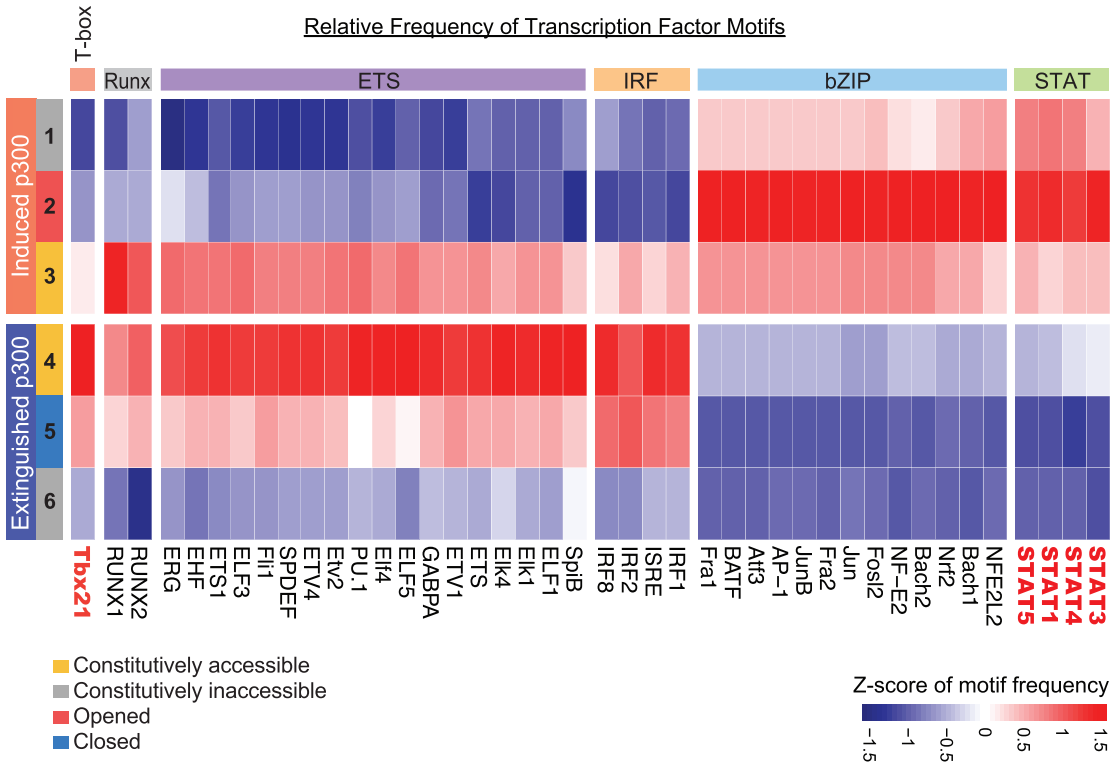

Figure 4. TF Motif Profiles Define Differential Drivers of Dynamic Enhancer Activities

Heatmap showing relative frequency of TF consensus motifs among six different enhancer classes defined in Figure 2A. Main TF families are highlighted at the top. The motif analysis was performed by HOMER and plotted by R.

between SRTFs acting at primed enhancers developmentally generated by T-bet/ETS/IRF/Runx families but also targeting of new regulatory regions to initiate *de novo* active enhancer landscape formation seemingly independent of LDTFs.

STAT4 Is Essential for Accessibility at *De Novo* Enhancers

Epigenomic landscapes define cellular identity and are established via the action of multiple factors, including LDTFs, pioneer TFs, and other co-factors that are thought to profoundly influence chromatin states (Heinz and Glass, 2012). Our previous data and the data provided herein point to the role of STATs in shaping the active enhancer landscapes of lymphocytes (Vahedi et al., 2012). However, it remains unclear as to how SRTFs affect accessibility and how this relates to formation of complex enhancer landscapes and rapid gene expression. To tackle this question, we analyzed the dynamics of p300 binding and accessibility in STAT-deficient NK cells upon activation. Stimulation with IL-12 and IL-2 is known to utilize STAT4 and STAT5 signaling pathways, respectively; however, STAT5 deficiency is not compatible with intact NK cell development and survival (Eckelhart et al., 2011; Stabile et al., 2018; Yao et al., 2006). Therefore, we focused on the analysis of NK cells isolated from *Stat4*$^{-/-}$ mice, which produce mature NK cells (Kaplan et al., 1996; Miyagi et al., 2007).

We found that among pre-bound p300 sites identified in Figure 2A, only 20% relied on STAT4 (Figure 5A). On the other hand, nearly 60% of inducible p300 binding required STAT4 (Figure 5A). To further study the effect of STAT4, we compared p300 binding within each class of enhancers in wild-type (WT) and STAT4-deficient NK cells. This comparison revealed that STAT4 contributes to p300 recruitment in *de novo* (class 2) and evolving (class 1) enhancers and, to a lesser extent, primed enhancers (class 3; Figure 5B). *Furin* represents an example of a HIG that undergoes extensive STAT4-dependent chromatin remodeling in response to IL-2 and IL-12 co-stimulation (Figure 5C, left panel). Activation of NK cells induced new p300 binding and accessible regions at non-coding regions ~35 kb upstream of the *Furin* gene. These modifications were absent in IL-2/IL-12-activated STAT4-deficient or IL-2-stimulated NK cells, suggesting an essential role for STAT4 in controlling enhancer accessibility at selective genomic foci, and, in this respect, could be viewed to function as a pioneer-like factor. Moreover, our data provided evidence for a nonredundant role of STAT4 in initiating the formation of *de novo* accessible, active enhancers in a sequence-dependent manner, despite the similarity of STAT4 and STAT5 motifs. Notably, although IL-12 alone was sufficient to open the chromatin, co-stimulation of IL-2 and IL-12 induced *Furin* expression to a higher extent (Figure S4C), indicating a cooperative effect of STAT4 and STAT5 for gene regulation beyond chromatin accessibility. Other STAT4-dependent *de novo* enhancers were also detected among intronic and intergenic regions as shown in Figures S5A and S5B. In contrast, another HIG, *AA467197*, represented an example of recruitment of p300 to compact

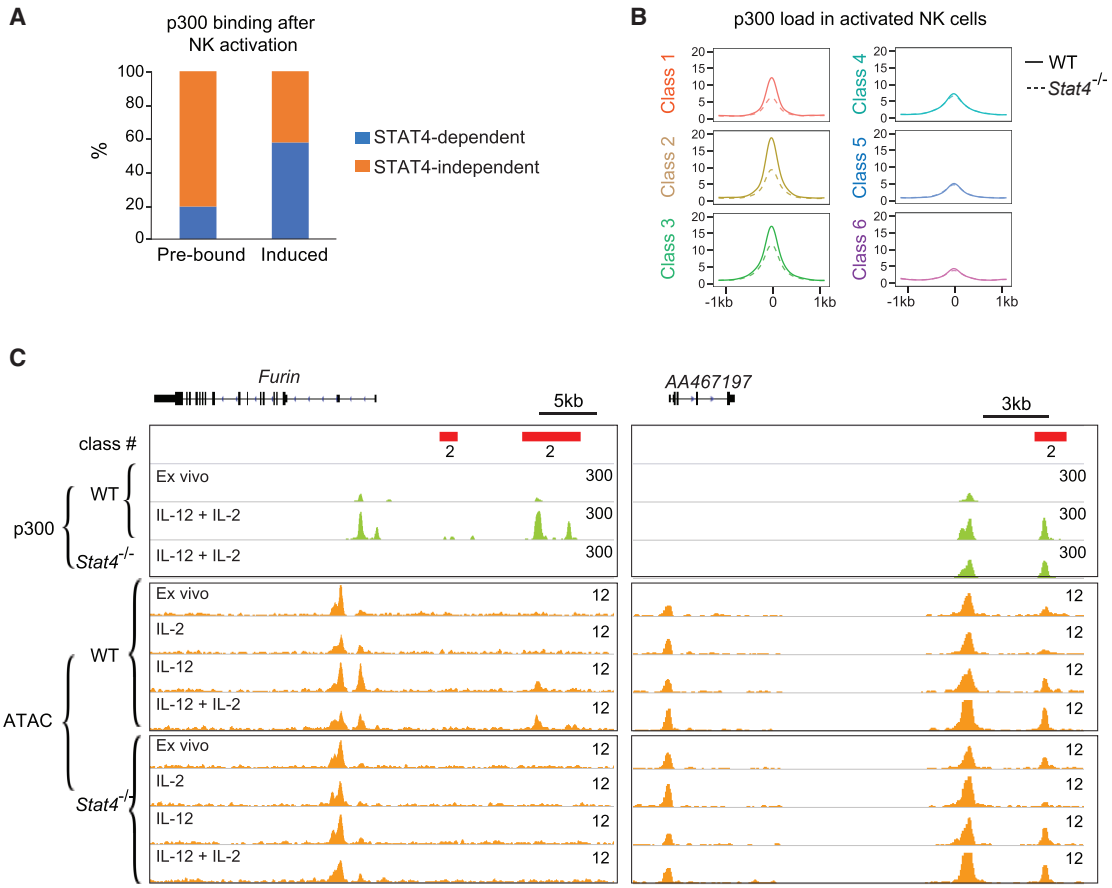

Figure 5. Formation of *De Novo* Enhancers Are Signal and TF Specific

(A) Frequency of STAT4-dependent p300 load after NK cell activation. p300 peaks from activated WT NK cells were first separated as pre-bound and newly induced based on p300 peak presence before and after cytokine stimulation. The STAT4 dependency was further determined by their presence (independent) or absence (dependent) in activated *Stat4*$^{-/-}$ NK cells.

(B) Analysis of STAT4 dependency for p300 load at six major enhancer classes defined in Figure 2A. Histogram plot depicts average distribution of p300 load around the center of inducible p300 peaks (±1 kb) in activated WT and *Stat4*$^{-/-}$ NK cells.

(C) Genomic snapshots showing p300 load and chromatin accessibility of WT and *Stat4*$^{-/-}$ NK cells treated with IL-12 and/or IL-2 at *Furin* and *AA467197* loci. See also Figure S5.

chromatin regions may be independent of STAT4 (Figure 5C, right panel).

Altogether, our data argue that STAT proteins rapidly change the enhancer landscapes in activated NK cells not only by targeting and activating primed enhancers but also by driving accessibility and forming *de novo* active enhancers. These epigenetic modifications collectively generate high-density p300-bound regions that are associated with rapid, high-level gene induction.

SRTFs Redeploy LDTFs to Non-canonical sites for High-Density p300 Focus Formation

To understand the roles of SRTFs and LDTFs in chromatin accessibility, formation of active enhancers and gene induction in NK cells, we next globally profiled binding sites for STAT4, STAT5, and T-bet using chromatin immunoprecipitation sequencing (ChIP-seq), comparing these regions to the identified enhancer classes. Consistent with our previous work in CD4^{+} T lymphocytes (Vahedi et al., 2012; Wei et al., 2010), we found STAT proteins preferentially bind non-promoter regions (Figure S6A) and are highly associated with inducible p300 binding (Figures 6A and 6B, classes 1–3); notably, this was evident in regions with prior and *de novo* accessibility. In line with this, nearly all p300 binding sites were bound by STAT4 (91%) (Figure S6B). On the other hand, STAT5 and T-bet bound to primed/poised enhancers (class 3) prior to stimulation and to class 1 and 2 enhancer regions upon NK activation (Figures 6A and 6B). The finding of T-bet binding to class 1 and 2 regulatory elements was unexpected as the motif analysis in Figure 4 indicated a scarcity of T-bet motif sequences in evolving (class 1) and *de novo* (class 2) enhancers. Prompted by this observation, we quantitated T-bet gene expression level and genome-wide occupancy upon NK stimulation (Figures S6C and S6D) and found that the redistribution of T-bet binding was not due to the alterations in T-bet expression or total number of T-bet peaks.

Pioneer factors create chromatin accessibility and in so doing permit the binding and action of other TFs on these genomic regions (Zaret and Carroll, 2011). Conventionally, LDTFs function as pioneer factors licensing SRTFs binding to regions opened

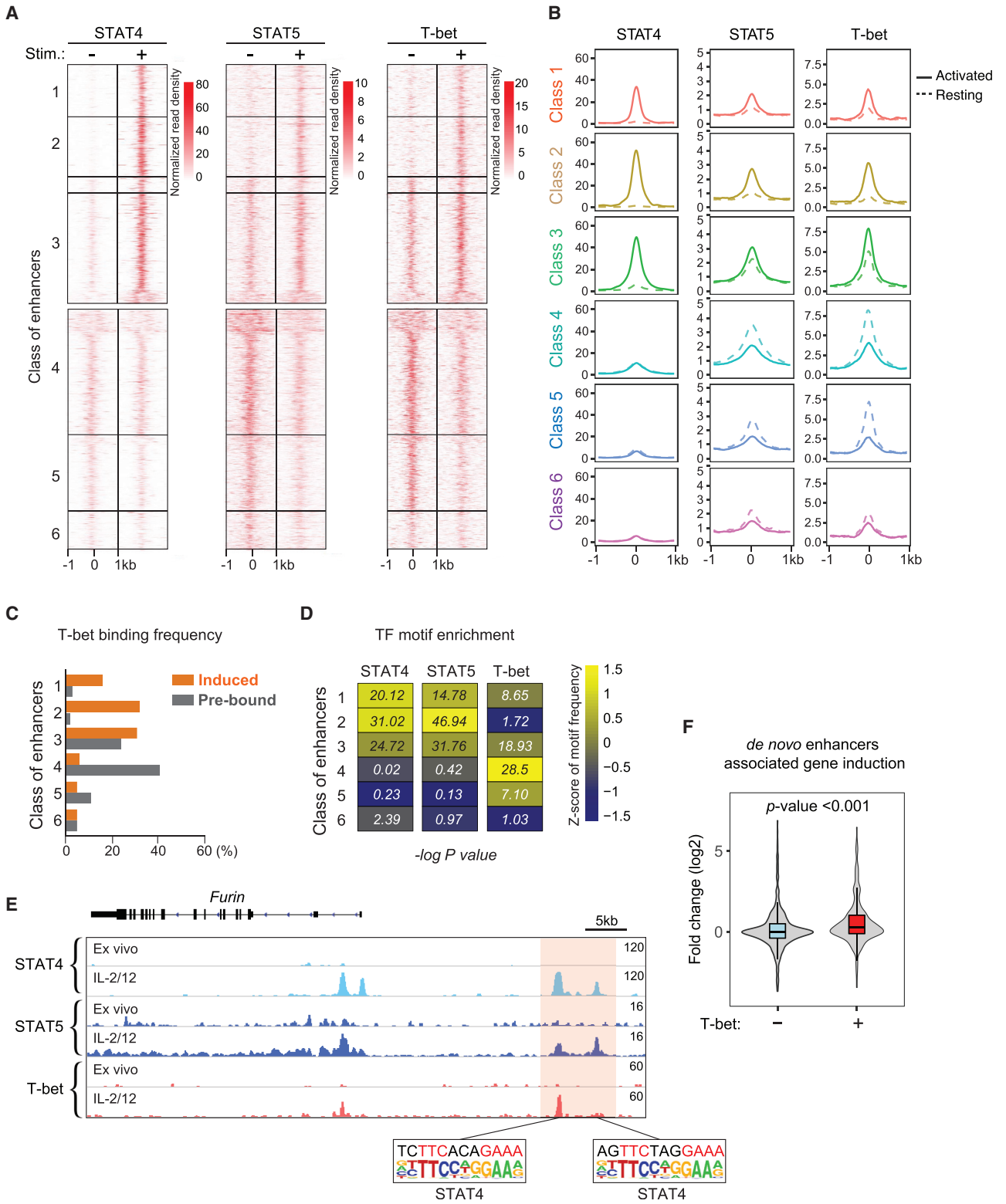

Figure 6. Global Redistribution of TFs Facilitates Rapid Gene Induction

(A) Peak density heatmap showing STAT4, STAT5, and T-bet binding at six enhancer classes defined in Figure 2A in resting and activated NK cells.

(B) Histogram plot depicts average distribution of STAT4, STAT5 and T-bet binding around the center of inducible p300 peaks (±1 kb) in resting and activated NK cells at six dynamic enhancer classes defined in Figure 2A.

(C) Frequency of T-bet binding among each enhancer class defined in Figure 2A in activated NK cells.

(legend continued on next page)

by LDTFs (Heinz et al., 2015). In macrophages, SRTFs contribute to the formation of *de novo* enhancers, which allow an LDTF (in this case, Pu.1) to engage its cognate DNA-binding motif (Kaikkonen et al., 2013; Ostuni et al., 2013).

To better understand the interactions between LDTFs and SRTFs in our system, we first identified T-bet-bound peaks in six enhancer classes (Figure 6C). We noted that prior to activation, prominent T-bet binding was demonstrable in regions with constitutive accessibility (classes 3 and 4). However, after activation, there was a major shift in localization of T-bet to regions that acquired accessibility (class 1 and 2 enhancers, along with class 3 regions). Next, we quantified the colocalization of T-bet and STAT proteins and found >95% colocalization in class 2–4 enhancers following activation (Figure S6E). We next compared DNA sequences among T-bet peaks in six enhancer classes for TF motifs (Figure 6D). We found that T-bet motifs were enriched among class 4 T-bet peaks ($p = 10^{-28.5}$) but were relatively rare among class 2 enhancers ($p = 10^{-1.72}$). By contrast, these regions were enriched for STAT motifs ($p = 10^{-31.02}$ and $10^{-46.94}$), STAT4 and STAT5 respectively, suggesting that STAT proteins direct T-bet recruitment at these regions. In contrast, T-bet binding in class 3 was enriched for both T-bet and STAT motifs. As exemplified by *Furin*, a locus with *de novo* enhancers as shown in Figure 5C, recruits SDTFs, such as STAT4 and STAT5, as well as LDTFs, such as T-bet, despite the fact that these regions possess STAT4, but not T-bet, motifs (Figure 6E). These enhancers evidently depend upon the IL-12 - STAT4 signaling axis for chromatin accessibility and p300 recruitment (Figure 5D). Similarly, inducible recruitment of T-bet also appeared on other *de novo* enhancers (class 2), exemplified by *Gcnt1* and *Prn* loci (Figure S6F). The loss of T-bet at enhancer classes 4–6 was exemplified by the *Cxcr4* locus (Figures 6B, 6D, and S6F).

We next sought to understand the relationships between the redeployment of T-bet to *de novo* enhancers and transcription activities. We found that the *de novo* enhancers associated with inducible T-bet peaks exhibited higher levels of gene induction compared to those without T-bet recruitment (Figure 6F). Collectively, our data indicate that cytokine signaling repurposes homeostatic T-bet binding, redistributing it to sites linked to high-level induction of gene expression via non-canonical DNA interactions. These results argue that STATs (SRTFs) function as pioneer factors that allow recruitment of p300 and other factors, including T-bet (LDTF), to establish new high-density p300 sites that can facilitate HIGs during an immune response; this occurs by non-canonical binding of T-bet.

DISCUSSION

The hardwired function of ILCs relies on developmental epigenetic programs enabling the selective priming of DNA regulatory elements related to effector genes (Lim et al., 2017; Shih et al., 2016). These programs also establish high-density enhancer structures associated with the distinct ILC functionalities (Collins et al., 2019; Koues et al., 2016). Herein, by integrating genomic measurements, we systematically and comprehensively surveyed how the enhancer landscape is integrated with the rapid transcriptional burst typical of innate lymphocytes and propose molecular mechanisms that control cascades of enhancer activation.

Our genome-wide analysis revealed that during activation, NK cells rapidly establish enhancer landscapes that differ from those generated during development. This is the result of cytokine-mediated changes occurring during activation and promoting p300 recruitment, histone and chromatin modifications leading to the formation of high-density enhancer landscapes near HIGs that are induced over 5-fold after stimulation. Sequential changes of chromatin accessibility in NK cells have been comprehensively evaluated during the acquisition of adaptive functions in the context of MCMV infection (Lau et al., 2018). Further, the remodeling of the *Il10* locus observed in NK cells during infection or the *Ifng* locus in type 3 ILCs represent good examples of how chronic stimulation can change chromatin accessibility (Mikami et al., 2018; Tarrio et al., 2014). Here, in the context of acute stimulation, accessibility changes and *de novo* enhancers formed rapidly in NK cells, after just 6 h of activation *in vitro*, and thus, represent an early event during NK immune response to *T. gondii* infection.

Our global TF-binding profiles revealed a massive distribution of STATs across the total high-density p300 sites (>95%) upon acute activation, concurrent with remodeling of NK cell enhancer landscapes. Formation of *de novo* enhancers and activation of primed enhancers was nearly abrogated in *Stat4*$^{-/-}$ NK cells, indicating the nonredundant roles for STATs in establishing enhancers during NK cell activation. Our data also point to a more complex usage of TFs during NK cell activation. Indeed, motif analysis approach revealed that *de novo* enhancers were enriched not only for STAT motifs but also for motifs for other TFs (such as AP-1 and Bach motifs), which could cooperate with STATs in promoting changes in the enhancer landscape. It is also important to consider that beyond STATs, IL-2 and IL-15 transmit their signals by engaging mTOR and mitogen-activated protein kinase (MAPK) pathways (Huntington et al., 2007; Mao et al., 2016; Marçais et al., 2014). The phosphatidylinositol 3-kinase (PI3K)-Akt-mTOR pathway is generally thought to influence gene expression/function by controlling mRNA dynamics (translation or degradation) and/or protein synthesis. The kinetics of these mechanisms may be insufficient to impact the transcriptional response described herein; however, kinases within the PI3K-Akt-mTOR pathway could mediate phosphorylation of TFs (e.g., polymerase II complex, mediator complex, and Myc), epigenetic regulators (i.e., histone acetylases and methyl transferases), and/or associated proteins (e.g., histones), which could be involved in rapid transcriptional effects. Likewise, other

(D) Heatmap showing relative frequency of STAT and T-bet consensus motifs among each enhancer class defined in Figure 2A. −log p value of TF motif enrichment within defined peaks were shown. See Table S4 for sequences and location of TF motifs.
(E) Genomic snapshot of STAT4, STAT5, and T-bet ChIP-seq analysis at *Furin* locus. Orange shade highlights genomic regions of *de novo* enhancers where STAT4, STAT5, and T-bet co-localize on a STAT4 consensus motif.
(F) Dynamic transcription activities of genes associated with *de novo* enhancers that recruit the NK cell LDTF T-bet.
See also Figure S6.

signaling pathways downstream of IL-2, particularly Ras-Raf-MAPK and ERK1/2, could propagate direct phosphorylation events that may also influence the rate of transcriptional changes described.

As T cell and ILC DNA-accessibility profiles converge following infection (Shih et al., 2016; Lau et al., 2018) and SRTFs dominate the enhancer usages in differentiated T cells rather than LDTFs (Vahedi et al., 2012), precise coordination and interplay between these TFs appears to be critical for mounting proper immune response. Here, we showed that the formation of accessible sites and enhancers driven by STATs was also associated with the redistribution of the LDTF T-bet. Thus, in acute activation, the canonical relationship between LDTFs and SRTFs is reversed. The conventional view is that LDTFs serve as pioneer factors to open inaccessible chromatin and facilitate deposition of SRTFs, which contribute to the transcriptional changes (Heinz et al., 2015). However, in the case of cytokine-stimulated ILCs, SRTFs also alter chromatin accessibility and, importantly, cause redeployment of the LDTF. In the case of T-bet, its total levels do not change, but activation results in its binding to many genomic regions, which are associated HIGs. These *de novo* T-bet peaks do not occur at genomic regions enriched for its canonical DNA motifs; rather, T-bet-bound regions are enriched for STAT-binding motifs, illustrating a new dominant role for well-known SRTFs like the STATs to guide preexisting LDTFs.

Limitations of Study

The genomic redistribution of LDTFs, such as T-bet, in activated NK cells opens the question of how the LDTFs are recruited to the new enhancers and whether this recruitment mediates rapid transcriptomic and epigenomic changes. Loss-of-function studies would be ideal to determine the relative importance of T-bet and other LDTFs in the regulation of highly dynamic genes in NK cells. However, germline deletion of T-bet blocks NK cell terminal maturation, and tamoxifen-induced conditional T-bet elimination results in incomplete NK maturation (Townsend et al., 2004; Madera et al., 2018). In addition, we found that T-bet expression persisted after 10 days of tamoxifen-induced gene deletion, suggesting that the half-life of the T-bet protein is long. Therefore, at present, the genomic tools available to examine the role of T-bet in activated NK cells are inadequate. Further, elucidating the molecular mechanisms behind how STATs affect the LDTF redistribution remains important.

STAR★METHODS

Detailed methods are provided in the online version of this paper and include the following:

- KEY RESOURCES TABLE
- RESOURCE AVAILABILITY
  - Lead Contact
  - Materials Availability
  - Data and Code Availability
- EXPERIMENTAL MODEL AND SUBJECT DETAILS
- METHOD DETAILS
  - Cell isolation, flow cytometry and *in vitro* stimulation
  - Bulk RNA sequencing
  - Single Cell RNA-Seq
  - ATAC-Seq
  - FastATAC-Seq
  - Chromatin Immunoprecipitation Sequencing (ChIP-Seq)
- QUANTIFICATION AND STATISTICAL ANALYSIS
  - Bioinformatics
  - RNA-Seq analysis
  - ChIP-Seq analysis
  - High-density p300 enhancer analysis
  - ATAC-Seq analysis
  - Classification of enhancers with dynamic chromatin accessibility and activity
  - scRNA-Seq analysis
  - Transcription factor motif analysis
  - Statistical analysis

SUPPLEMENTAL INFORMATION

Supplemental Information can be found online at https://doi.org/10.1016/j.immuni.2020.09.008.

ACKNOWLEDGMENTS

We thank S. Dell'Orso, G. Gutierrez-Cruz (Genomic Technology Section, NIAMS), J. Simone, J. Lay, and K. Tinsley (Flow Cytometry Section, NIAMS) for their excellent technical support. We thank Dr. Nilisha Fernando for proofreading this manuscript. This study utilized the high-performance computational capabilities of the Biowulf Linux cluster at the NIH. This work was supported by the Intramural Research Programs of the NEI, NIAMS, and NIAID and the Italian Association for Cancer Research (AIRC) (MFAG 2018; project code 21311).

AUTHOR CONTRIBUTIONS

Conceptualization, G.S., Y.K., J.J.O., and H.-Y.S.; Writing – Original Draft, G.S., J.J.O., and H.-Y.S.; Writing – Review & Editing, G.S., V.S., Y.K., J.J.O., and H.-Y.S.; Investigation, G.S., Y.M., D.J., H.N., A.V., T.M., C.Y., S.S., D.F., S.N., K.H., B.Z., Y.K., and H.-Y.S.; Formal Analysis, H.-W.S., S.R.B., F.P.D., and H.-Y.S.

DECLARATION OF INTERESTS

The authors declare no competing interests.

Received: October 29, 2019
Revised: May 8, 2020
Accepted: September 11, 2020
Published: October 2, 2020

REFERENCES

Barton, K., Muthusamy, N., Fischer, C., Ting, C.N., Walunas, T.L., Lanier, L.L., and Leiden, J.M. (1998). The Ets-1 transcription factor is required for the development of natural killer cells in mice. Immunity *9*, 555–563.

Bezman, N.A., Kim, C.C., Sun, J.C., Min-Oo, G., Hendricks, D.W., Kamimura, Y., Best, J.A., Goldrath, A.W., and Lanier, L.L.; Immunological Genome Project Consortium (2012). Molecular definition of the identity and activation of natural killer cells. Nat. Immunol. *13*, 1000–1009.

Bonelli, M., Shih, H.-Y., Hirahara, K., Singelton, K., Laurence, A., Poholek, A., Hand, T., Mikami, Y., Vahedi, G., Kanno, Y., and O'Shea, J.J. (2014). Helper T cell plasticity: impact of extrinsic and intrinsic signals on transcriptomes and epigenomes. Curr. Top. Microbiol. Immunol. *381*, 279–326.

Buenrostro, J.D., Giresi, P.G., Zaba, L.C., Chang, H.Y., and Greenleaf, W.J. (2013). Transposition of native chromatin for fast and sensitive epigenomic

profiling of open chromatin, DNA-binding proteins and nucleosome position. Nat. Methods *10*, 1213–1218.

Butler, A., Hoffman, P., Smibert, P., Papalexi, E., and Satija, R. (2018). Integrating single-cell transcriptomic data across different conditions, technologies, and species. Nat. Biotechnol. *36*, 411–420.

Choi, H.-J., Geng, Y., Cho, H., Li, S., Giri, P.K., Felio, K., and Wang, C.-R. (2011). Differential requirements for the Ets transcription factor Elf-1 in the development of NKT cells and NK cells. Blood *117*, 1880–1887.

Collins, P.L., Cella, M., Porter, S.I., Li, S., Gurewitz, G.L., Hong, H.S., Johnson, R.P., Oltz, E.M., and Colonna, M. (2019). Gene regulatory programs conferring phenotypic identities to human NK cells. Cell *176*, 348–360.e12.

Corces, M.R., Buenrostro, J.D., Wu, B., Greenside, P.G., Chan, S.M., Koenig, J.L., Snyder, M.P., Pritchard, J.K., Kundaje, A., Greenleaf, W.J., et al. (2016). Lineage-specific and single-cell chromatin accessibility charts human hematopoiesis and leukemia evolution. Nat. Genet. *48*, 1193–1203.

Diefenbach, A., Colonna, M., and Koyasu, S. (2014). Development, differentiation, and diversity of innate lymphoid cells. Immunity *41*, 354–365.

Ebihara, T., Song, C., Ryu, S.H., Plougastel-Douglas, B., Yang, L., Levanon, D., Groner, Y., Bern, M.D., Stappenbeck, T.S., Colonna, M., et al. (2015). Runx3 specifies lineage commitment of innate lymphoid cells. Nat. Immunol. *16*, 1124–1133.

Eckelhart, E., Warsch, W., Zebedin, E., Simma, O., Stoiber, D., Kolbe, T., Rülicke, T., Mueller, M., Casanova, E., and Sexl, V. (2011). A novel Ncr1-Cre mouse reveals the essential role of STAT5 for NK-cell survival and development. Blood *117*, 1565–1573.

Furlong, E.E.M., and Levine, M. (2018). Developmental enhancers and chromosome topology. Science *361*, 1341–1345.

Garber, M., Yosef, N., Goren, A., Raychowdhury, R., Thielke, A., Guttman, M., Robinson, J., Minie, B., Chevrier, N., Itzhaki, Z., et al. (2012). A high-throughput chromatin immunoprecipitation approach reveals principles of dynamic gene regulation in mammals. Mol. Cell *47*, 810–822.

Glass, C.K., and Natoli, G. (2016). Molecular control of activation and priming in macrophages. Nat. Immunol. *17*, 26–33.

Goldszmid, R.S., Caspar, P., Rivollier, A., White, S., Dzutsev, A., Hieny, S., Kelsall, B., Trinchieri, G., and Sher, A. (2012). NK cell-derived interferon-γ orchestrates cellular dynamics and the differentiation of monocytes into dendritic cells at the site of infection. Immunity *36*, 1047–1059.

Gury-BenAri, M., Thaiss, C.A., Serafini, N., Winter, D.R., Giladi, A., Lara-Astiaso, D., Levy, M., Salame, T.M., Weiner, A., David, E., et al. (2016). The spectrum and regulatory landscape of intestinal innate lymphoid cells are shaped by the microbiome. Cell *166*, 1231–1246.e13.

Heinz, S., and Glass, C.K. (2012). Roles of lineage-determining transcription factors in establishing open chromatin: lessons from high-throughput studies. Curr. Top. Microbiol. Immunol. *356*, 1–15.

Heinz, S., Benner, C., Spann, N., Bertolino, E., Lin, Y.C., Laslo, P., Cheng, J.X., Murre, C., Singh, H., and Glass, C.K. (2010). Simple combinations of lineage-determining transcription factors prime cis-regulatory elements required for macrophage and B cell identities. Mol. Cell *38*, 576–589.

Heinz, S., Romanoski, C.E., Benner, C., and Glass, C.K. (2015). The selection and function of cell type-specific enhancers. Nat. Rev. Mol. Cell Biol. *16*, 144–154.

Hnisz, D., Abraham, B.J., Lee, T.I., Lau, A., Saint-André, V., Sigova, A.A., Hoke, H.A., and Young, R.A. (2013). Super-enhancers in the control of cell identity and disease. Cell *155*, 934–947.

Hnisz, D., Day, D.S., and Young, R.A. (2016). Insulated neighborhoods: structural and functional units of mammalian gene control. Cell *167*, 1188–1200.

Huntington, N.D., Puthalakath, H., Gunn, P., Naik, E., Michalak, E.M., Smyth, M.J., Tabarias, H., Degli-Esposti, M.A., Dewson, G., Willis, S.N., et al. (2007). Interleukin 15-mediated survival of natural killer cells is determined by interactions among Bim, Noxa and Mcl-1. Nat. Immunol. *8*, 856–863.

Kaikkonen, M.U., Spann, N.J., Heinz, S., Romanoski, C.E., Allison, K.A., Stender, J.D., Chun, H.B., Tough, D.F., Prinjha, R.K., Benner, C., and Glass, C.K. (2013). Remodeling of the enhancer landscape during macrophage activation is coupled to enhancer transcription. Mol. Cell *51*, 310–325.

Kaplan, M.H., Sun, Y.L., Hoey, T., and Grusby, M.J. (1996). Impaired IL-12 responses and enhanced development of Th2 cells in Stat4-deficient mice. Nature *382*, 174–177.

Koues, O.I., Collins, P.L., Cella, M., Robinette, M.L., Porter, S.I., Pyfrom, S.C., Payton, J.E., Colonna, M., and Oltz, E.M. (2016). Distinct gene regulatory pathways for human innate versus adaptive lymphoid cells. Cell *165*, 1134–1146.

Kugler, D.G., Mittelstadt, P.R., Ashwell, J.D., Sher, A., and Jankovic, D. (2013). CD4+ T cells are trigger and target of the glucocorticoid response that prevents lethal immunopathology in toxoplasma infection. J. Exp. Med. *210*, 1919–1927.

Lacorazza, H.D., Miyazaki, Y., Di Cristofano, A., Deblasio, A., Hedvat, C., Zhang, J., Cordon-Cardo, C., Mao, S., Pandolfi, P.P., and Nimer, S.D. (2002). The ETS protein MEF plays a critical role in perforin gene expression and the development of natural killer and NK-T cells. Immunity *17*, 437–449.

Langmead, B., Trapnell, C., Pop, M., and Salzberg, S.L. (2012). Ultrafast and memory-efficient alignment of short DNA sequences to the human genome. Genome Biol *10*, R25.

Lau, C.M., Adams, N.M., Geary, C.D., Weizman, O.-E., Rapp, M., Pritykin, Y., Leslie, C.S., and Sun, J.C. (2018). Epigenetic control of innate and adaptive immune memory. Nat. Immunol. *19*, 963–972.

Lim, A.I., Li, Y., Lopez-Lastra, S., Stadhouders, R., Paul, F., Casrouge, A., Serafini, N., Puel, A., Bustamante, J., Surace, L., et al. (2017). Systemic human ILC precursors provide a substrate for tissue ILC differentiation. Cell *168*, 1086–1100.e10.

Lovén, J., Hoke, H.A., Lin, C.Y., Lau, A., Orlando, D.A., Vakoc, C.R., Bradner, J.E., Lee, T.I., and Young, R.A. (2013). Selective inhibition of tumor oncogenes by disruption of super-enhancers. Cell *153*, 320–334.

Macosko, E.Z., Basu, A., Satija, R., Nemesh, J., Shekhar, K., Goldman, M., Tirosh, I., Bialas, A.R., Kamitaki, N., Martersteck, E.M., et al. (2015). Highly parallel genome-wide expression profiling of individual cells using nanoliter droplets. Cell *161*, 1202–1214.

Madera, S., Geary, C.D., Lau, C.M., Pikovskaya, O., Reiner, S.L., and Sun, J.C. (2018). Cutting edge: divergent requirement of T-Box transcription factors in effector and memory NK cells. J. Immunol. *200*, 1977–1981.

Mao, Y., van Hoef, V., Zhang, X., Wennerberg, E., Lorent, J., Witt, K., Masvidal, L., Liang, S., Murray, S., Larsson, O., et al. (2016). IL-15 activates mTOR and primes stress-activated gene expression leading to prolonged antitumor capacity of NK cells. Blood *128*, 1475–1489.

Marçais, A., Viel, S., Grau, M., Henry, T., Marvel, J., and Walzer, T. (2013). Regulation of mouse NK cell development and function by cytokines. Front. Immunol. *4*, 450.

Marçais, A., Cherfils-Vicini, J., Viant, C., Degouve, S., Viel, S., Fenis, A., Rabilloud, J., Mayol, K., Tavares, A., Bienvenu, J., et al. (2014). The metabolic checkpoint kinase mTOR is essential for IL-15 signaling during the development and activation of NK cells. Nat. Immunol. *15*, 749–757.

Mikami, Y., Scarno, G., Zitti, B., Shih, H.-Y., Kanno, Y., Santoni, A., O'Shea, J.J., and Sciumè, G. (2018). NCR$^+$ ILC3 maintain larger STAT4 reservoir via T-BET to regulate type 1 features upon IL-23 stimulation in mice. Eur. J. Immunol. *48*, 1174–1180.

Miyagi, T., Gil, M.P., Wang, X., Louten, J., Chu, W.-M., and Biron, C.A. (2007). High basal STAT4 balanced by STAT1 induction to control type 1 interferon effects in natural killer cells. J. Exp. Med. *204*, 2383–2396.

Ostuni, R., Piccolo, V., Barozzi, I., Polletti, S., Termanini, A., Bonifacio, S., Curina, A., Prosperini, E., Ghisletti, S., and Natoli, G. (2013). Latent enhancers activated by stimulation in differentiated cells. Cell *152*, 157–171.

Phan, A.T., Goldrath, A.W., and Glass, C.K. (2017). Metabolic and epigenetic coordination of T cell and macrophage immunity. Immunity *46*, 714–729.

Pope, S.D., and Medzhitov, R. (2018). Emerging principles of gene expression programs and their regulation. Mol. Cell *71*, 389–397.

Quinlan, A.R., and Hall, I.M. (2010). BEDTools: a flexible suite of utilities for comparing genomic features. Bioinformatics *26*, 841–842.

Rapp, M., Lau, C.M., Adams, N.M., Weizman, O.-E., O'Sullivan, T.E., Geary, C.D., and Sun, J.C. (2017). Core-binding factor β and Runx transcription factors promote adaptive natural killer cell responses. Sci. Immunol. *2*, 2.

Robinette, M.L., Fuchs, A., Cortez, V.S., Lee, J.S., Wang, Y., Durum, S.K., Gilfillan, S., Colonna, M., Shaw, L., Yu, B., et al.; Immunological Genome Consortium (2015). Transcriptional programs define molecular characteristics of innate lymphoid cell classes and subsets. Nat. Immunol. *16*, 306–317.

Sciumè, G., Shih, H.-Y., Mikami, Y., and O'Shea, J.J. (2017). Epigenomic views of innate lymphoid cells. Front. Immunol. *8*, 1579.

Sher, A., Collazzo, C., Scanga, C., Jankovic, D., Yap, G., and Aliberti, J. (2003). Induction and regulation of IL-12-dependent host resistance to Toxoplasma gondii. Immunol. Res. *27*, 521–528.

Shih, H.-Y., Sciumè, G., Poholek, A.C., Vahedi, G., Hirahara, K., Villarino, A.V., Bonelli, M., Bosselut, R., Kanno, Y., Muljo, S.A., and O'Shea, J.J. (2014). Transcriptional and epigenetic networks of helper T and innate lymphoid cells. Immunol. Rev. *261*, 23–49.

Shih, H.-Y., Sciumè, G., Mikami, Y., Guo, L., Sun, H.W., Brooks, S.R., Urban, J.F., Jr., Davis, F.P., Kanno, Y., and O'Shea, J.J. (2016). Developmental acquisition of regulomes underlies innate lymphoid cell functionality. Cell *165*, 1120–1133.

Smale, S.T., and Natoli, G. (2014). Transcriptional control of inflammatory responses. Cold Spring Harb. Perspect. Biol. *6*, a016261.

Smale, S.T., Tarakhovsky, A., and Natoli, G. (2014). Chromatin contributions to the regulation of innate immunity. Annu. Rev. Immunol. *32*, 489–511.

Spits, H., Artis, D., Colonna, M., Diefenbach, A., Di Santo, J.P., Eberl, G., Koyasu, S., Locksley, R.M., McKenzie, A.N.J., Mebius, R.E., et al. (2013). Innate lymphoid cells–a proposal for uniform nomenclature. Nat. Rev. Immunol. *13*, 145–149.

Stabile, H., Scarno, G., Fionda, C., Gismondi, A., Santoni, A., Gadina, M., and Sciumè, G. (2018). JAK/STAT signaling in regulation of innate lymphoid cells: the gods before the guardians. Immunol. Rev. *286*, 148–159.

Stetson, D.B., Mohrs, M., Reinhardt, R.L., Baron, J.L., Wang, Z.-E., Gapin, L., Kronenberg, M., and Locksley, R.M. (2003). Constitutive cytokine mRNAs mark natural killer (NK) and NK T cells poised for rapid effector function. J. Exp. Med. *198*, 1069–1076.

Tarrio, M.L., Lee, S.-H., Fragoso, M.F., Sun, H.-W., Kanno, Y., O'Shea, J.J., and Biron, C.A. (2014). Proliferation conditions promote intrinsic changes in NK cells for an IL-10 response. J. Immunol. *193*, 354–363.

Tato, C.M., Martins, G.A., High, F.A., DiCioccio, C.B., Reiner, S.L., and Hunter, C.A. (2004). Cutting Edge: Innate production of IFN-gamma by NK cells is independent of epigenetic modification of the IFN-gamma promoter. J. Immunol. *173*, 1514–1517.

Tong, A.-J., Liu, X., Thomas, B.J., Lissner, M.M., Baker, M.R., Senagolage, M.D., Allred, A.L., Barish, G.D., and Smale, S.T. (2016). A stringent systems approach uncovers gene-specific mechanisms regulating inflammation. Cell *165*, 165–179.

Townsend, M.J., Weinmann, A.S., Matsuda, J.L., Salomon, R., Farnham, P.J., Biron, C.A., Gapin, L., and Glimcher, L.H. (2004). T-bet regulates the terminal maturation and homeostasis of NK and Valpha14i NKT cells. Immunity *20*, 477–494.

Trapnell, C., Roberts, A., Goff, L., Pertea, G., Kim, D., Kelley, D.R., Pimentel, H., Salzberg, S.L., Rinn, J.L., and Pachter, L. (2012). Differential gene and transcript expression analysis of RNA-seq experiments with TopHat and Cufflinks. Nat. Protoc. *7*, 562–578.

Vahedi, G., Takahashi, H., Nakayamada, S., Sun, H.-W., Sartorelli, V., Kanno, Y., and O'Shea, J.J. (2012). STATs shape the active enhancer landscape of T cell populations. Cell *151*, 981–993.

Vahedi, G., Kanno, Y., Furumoto, Y., Jiang, K., Parker, S.C.J., Erdos, M.R., Davis, S.R., Roychoudhuri, R., Restifo, N.P., Gadina, M., et al. (2015). Super-enhancers delineate disease-associated regulatory nodes in T cells. Nature *520*, 558–562.

Villarino, A.V., Sciumè, G., Davis, F.P., Iwata, S., Zitti, B., Robinson, G.W., Hennighausen, L., Kanno, Y., and O'Shea, J.J. (2017b). Subset- and tissue-defined STAT5 thresholds control homeostasis and function of innate lymphoid cells. J. Exp. Med. *214*, 2999–3014.

Vivier, E., Artis, D., Colonna, M., Diefenbach, A., Di Santo, J.P., Eberl, G., Koyasu, S., Locksley, R.M., McKenzie, A.N.J., Mebius, R.E., et al. (2018). Innate lymphoid cells: 10 years on. Cell *174*, 1054–1066.

Wei, L., Vahedi, G., Sun, H.-W., Watford, W.T., Takatori, H., Ramos, H.L., Takahashi, H., Liang, J., Gutierrez-Cruz, G., Zang, C., et al. (2010). Discrete roles of STAT4 and STAT6 transcription factors in tuning epigenetic modifications and transcription during T helper cell differentiation. Immunity *32*, 840–851.

Whyte, W.A., Orlando, D.A., Hnisz, D., Abraham, B.J., Lin, C.Y., Kagey, M.H., Rahl, P.B., Lee, T.I., and Young, R.A. (2013). Master transcription factors and mediator establish super-enhancers at key cell identity genes. Cell *153*, 307–319.

Winter, D.R., and Amit, I. (2014). The role of chromatin dynamics in immune cell development. Immunol. Rev. *261*, 9–22.

Witte, S., O'Shea, J.J., and Vahedi, G. (2015). Super-enhancers: asset management in immune cell genomes. Trends Immunol. *36*, 519–526.

Xu, H., Luo, X., Qian, J., Pang, X., Song, J., Qian, G., Chen, J., and Chen, S. (2012). FastUniq: a fast de novo duplicates removal tool for paired short reads. PLoS ONE *7*, e52249.

Yao, Z., Cui, Y., Watford, W.T., Bream, J.H., Yamaoka, K., Hissong, B.D., Li, D., Durum, S.K., Jiang, Q., Bhandoola, A., et al. (2006). Stat5a/b are essential for normal lymphoid development and differentiation. Proc. Natl. Acad. Sci. USA *103*, 1000–1005.

Zang, C., Schones, D.E., Zeng, C., Cui, K., Zhao, K., and Peng, W. (2009). A clustering approach for identification of enriched domains from histone modification ChIP-seq data. Bioinformatics *25*, 1952–1958.

Zaret, K.S., and Carroll, J.S. (2011). Pioneer transcription factors: establishing competence for gene expression. Genes Dev. *25*, 2227–2241.

Zhang, Y., Liu, T., MeyerEeckhoute, C.A.J., Johnson, D.S., Bernstein, B.E., Nusbaum, C., Myers, R.M., Brown, M., Li, W., et al. (2008). Model-based Analysis of ChIP-Seq (MACS). Genome Biol *9*, R137. https://doi.org/10.1186/gb-2008-9-9-r137.

Zhang, J., Marotel, M., Fauteux-Daniel, S., Mathieu, A.-L., Viel, S., Marçais, A., and Walzer, T. (2018). T-bet and Eomes govern differentiation and function of mouse and human NK cells and ILC1. Eur. J. Immunol. *48*, 738–750.

STAR★METHODS

KEY RESOURCES TABLE

REAGENT or RESOURCE	SOURCE	IDENTIFIER
Antibodies		
anti-CD3ε (clone: 145-2C11)	BD Biosciences	Cat# 561042, RRID: AB_2034003
anti-CD16/CD32 (2.4G2)	BD Biosciences	Cat# 553140, RRID: AB_394655
anti-NKp46 (29A1.4)	Thermo Fisher Scientific	Cat# 51-3351-82, RRID: AB_1257145
anti-CD49b (DX5)	BD Biosciences	Cat# 553855, RRID: AB_395091
anti-H3K27Ac	AbCam	Abcam Cat# ab4729, RRID: AB_2118291
anti-H3K4me3	Millipore	Cat# 04-745, RRID: AB_1163444
anti-H3K27me3	Millipore	Cat# 07-449, RRID: AB_310624
anti-H3K4me1	AbCam	Cat# ab8895, RRID: AB_306847
anti-p300	Santa Cruz	Cat# SC-585, RRID: AB_2231120
anti-STAT4	Santa Cruz	Cat# sc-486, RRID: AB_632444
anti-STAT5	AbCam	Cat# ab7969, RRID: AB_306183
anti-T-bet	Santa Cruz	Cat# sc-21003, RRID: AB_2200557
Chemicals, Peptides, and Recombinant Proteins		
Recombinant Human IL-2	NCI Biological Resources Branch	N/A
Recombinant Mouse IL-12	R&D	Cat# 419-ML
TRIzol	Life Technologies/ThermoFisher Scientific	Cat# 15596026
Critical Commercial Assays		
TruSeq SR mRNA sample prep kit	Illumina	FC-122-1001
Chromium Single Cell 3′ Reagent Kits v2	10X Genomics	CG00052
TDE1, Tagment DNA Enzyme	Illumina	15027865
TD, Tagment DNA Buffer	Illumina	15027866
NEBNext High-Fidelity 2x PCR Master Mix	New England Labs	Cat# M0541
Digitonin	Promega	G9441
Deposited Data		
Raw and analyzed data	This paper	GEO: GSE145299
Part of NK cell STAT5 ChIP-seq	Villarino et al., 2017b	GEO: GSE100674
Part of NK cell T-bet and p300 ChIP-seq and ATAC-seq	Shih et al., 2016	GEO: GSE77695
Experimental Models: Cell Lines		
Mouse: C57BL/6J	The Jackson Laboratory	JAX: 000664
Mouse: *Stat4*$^{-/-}$	The Jackson Laboratory	JAX: 002826
Experimental Models: Organisms/Strains		
T. gondii strain ME-49	Remington lab at Stanford	N/A
Oligonucleotides		
ATAC-seq indexed primers	Buenrostro et al., 2013	N/A
Software and Algorithms		
FlowJo software	Tree Star	https://www.flowjo.com/
Bowtie 0.12.8	Langmead et al., 2012	http://bowtie-bio.sourceforge.net/index.shtml
Homer v4.10	Heinz et al., 2010	http://homer.ucsd.edu/homer/
MACS 1.4.2	Zhang et al., 2008	https://bioweb.pasteur.fr/packages/pack@macs@1.4.2
Python 3.3.2	Python Software Foundation	https://www.python.org
R 3.4.0	R Development Core Team	https://www.R-project.org

(*Continued on next page*)

Continued

REAGENT or RESOURCE	SOURCE	IDENTIFIER
RStudio 1.0.143	RStudio Team	http://www.rstudio.com
SICER 1.1	Zang et al., 2009	
Igv 2.3.42	The Broad Institute	http://software.broadinstitute.org/software/igv/igv2.3
Partek Genomics Suite 6.6	Partek	https://www.partek.com/partek-genomics-suite/
Bedtools	Quinlan and Hall, 2010	https://bedtools.readthedocs.io/en/latest/
CASAVA 1.8.2	Illumina	https://bioweb.pasteur.fr/packages/pack@casava@1.8.2
TopHat 2.1.0	Trapnell et al., 2012	https://ccb.jhu.edu/software/tophat/index.shtml
Cufflinks 2.2.1	Trapnell et al., 2012	http://cole-trapnell-lab.github.io/cufflinks/
FastUniq	Xu et al., 2012	https://sourceforge.net/projects/fastuniq/files/
Seurat	Butler et al., 2018; Macosko et al., 2015	https://satijalab.org/seurat/

RESOURCE AVAILABILITY

Lead Contact

Further information and requests for resources and reagents should be directed to and will be fulfilled by the Lead Contact, Han-Yu Shih (han-yu.shih@nih.gov).

Materials Availability

This study did not generate new unique reagents.

Data and Code Availability

The ATAC-seq, RNA-seq, and ChIP-seq data have been deposited in the GEO: GSE145299.

EXPERIMENTAL MODEL AND SUBJECT DETAILS

Female wild-type C57BL/6J (6- to 12-week-old) were purchased from Jackson Laboratory. *Stat4*$^{-/-}$ mice were kindly provided by M Kaplan (Kaplan et al., 1996). For experiments involving *T. gondii* infection, mice of at least 8 weeks of age were inoculated with an average of 15 cysts of type II avirulent *T. gondii* strain ME-49 by intraperitoneal injection (Kugler et al., 2013). All animal studies were performed according to the National Institutes of Health guidelines for the use and care of live animals and were approved by the Institutional Animal Care and Use Committee of the National Institute of Arthritis, Musculoskeletal and Skin Diseases and National Eye Institute.

METHOD DETAILS

Cell isolation, flow cytometry and *in vitro* stimulation

Cells were isolated from spleens by mechanical disruption. Peritoneal cells were obtained by washing of the peritoneal cavity with cold PBS. For transcriptomic analyses, NK cells were FACS-sorted as CD3ε^{-}NKp46^{+}CD49b^{+} cells using FACS-Aria III (BD), as described previously (Shih et al., 2016; Villarino et al., 2017b). For ChIP-Seq experiments, splenocytes from mice were first pooled and enriched by Ficoll. Next, NK cells were enriched by negative selection (Miltenyi), and FACS-sorted as CD3ε^{-}NKp46^{+} cells. Cell surface staining was performed with anti-mouse CD3ε (145-2C11), CD16/CD32 (2.4G2), CD49b (DX5) and NKp46 (29A1.4). Samples were acquired using FACSVerse or FACSCanto (BD Biosciences) and analyzed with FlowJo software (Tree Star). Sorted NK cells were stimulated with IL-2 (1000 U/ml) and/or IL-12 (10 ng/ml, R&D) in RPMI medium with 10% (vol/vol) FCS (Invitrogen), 2 mM glutamine (Invitrogen), 100 IU/ml penicillin (Invitrogen), 0.1 mg/ml streptomycin (Invitrogen), and 20 mM HEPES buffer, pH 7.2–7.5 (Invitrogen), and 2 mM β-mercaptoethanol (Sigma-Aldrich) for 6 hours.

Bulk RNA sequencing

Total RNA was prepared from 50,000 cells by using TRIzol according to the manufacturer's protocol (Life Technologies). Next, total RNA was processed to a mRNA-Seq library using TruSeq SR mRNA sample prep kit (FC-122-1001, Illumina). The libraries were sequenced for 50 cycles (single read) with a HiSeq 2000 or HiSeq 2500 (Illumina).

Single Cell RNA-Seq

NK cells from spleen and peritoneal cavity were isolated after 0, 3 or 7 days of infection, as indicated in Figure 3A. Sorted NK cells (13,000 cells each, cell viability > 98%) were encapsulated into droplets, and libraries were prepared using Chromium Single Cell 3′ Reagent Kits v2 according to the manufacturer's protocol (10X Genomics). The generated scRNA-Seq libraries were sequenced using a 50 cycle (paired-end) with a HiSeq 3000 (Illumina).

ATAC-Seq

ATAC-Seq was performed according to a published protocol (Buenrostro et al., 2013) with minor modifications. 50,000 cells were pelleted and washed with 50 μl PBS, followed by treatment with 50 μl lysis buffer (10 mM Tris-HCl [pH 7.4], 10 mM NaCl, 3 mM MgCl2, 0.1% IGEPAL CA-630). After pelleting the nuclei by centrifuging at 500 x g for 10 min at 4°C, the pellets were re-suspended in a 40 μl transposition reaction with 2 μl Tn5 transposase (Illumina) to tag and fragmentalize accessible chromatin. The reaction was incubated at 37C with shaking at 300 rpm for 30 min. The fragmentalized DNAs were then purified using a QIAGEN MinElute kit and amplified with 10 or 11 cycles of PCR based on the amplification curve. Once the libraries were purified using a QIAGEN PCR cleanup kit, they were further sequenced for 50 cycles (paired-end reads) on a HiSeq 2500.

FastATAC-Seq

FastATAC-Seq was performed according to a published protocol with minor modifications (Corces et al., 2016). 10,000 cells were pelleted and washed with 50 μL PBS. After pelleting the nuclei by centrifuging at 500 x g for 10 min at 4°C, the pellets were re-suspended in 50 μL transposase mixture (25 μL of 2x TD buffer, 2.5 μL of TDE1, 0.5 μL of 1% digitonin, 22 μL of nuclease-free water) (see Key Resources Table). The reaction was incubated at 37°C with shaking at 300 rpm for 30 min. The remaining steps for DNA purification, amplification and sequencing were identical to ATAC-Seq described above.

Chromatin Immunoprecipitation Sequencing (ChIP-Seq)

ChIP-Seq was performed using at least 10 million sorted NK cells without or with cytokine stimulation. After chemically cross-linking cells, chromatin was fragmented by sonication and immunoprecipitated by anti-H3K27Ac (ab4729; Abcam), anti-H3K4me3 (04-745; Millipore), anti-H3K27me3 (07-449; Millipore), anti-H3K4me1 (ab8895; AbCam), anti-p300 (sc585; Santa Cruz), anti-STAT4 (sc486; Santa Cruz), anti-STAT5 (ab7969; AbCam) or anti-T-bet (sc21003; Santa Cruz). After recovering purified DNA, 10 ng or more of DNA was used to generate libraries according to the vendor's manual for the Illumina platform (E6240S/L; New England BioLabs). Illumina HiSeq 2500 or Genome Analyzer II was used for 50-cycle single-read sequencing.

QUANTIFICATION AND STATISTICAL ANALYSIS

Bioinformatics

The following software were used:

- Bowtie 0.12.8
- Homer v4.10 (Heinz et al., 2010)
- MACS 1.4.2
- Python 3.3.2 (https://www.python.org)
- R 3.4.0 (https://www.R-project.org)
- RStudio 1.0.143 (http://www.rstudio.com)
- SICER 1.1 (Zang et al., 2009)
- Igv 2.3.42
- Partek Genomics Suite 6.6
- Bedtools (Quinlan and Hall, 2010)
- Seurat (Butler et al., 2018)

RNA-Seq analysis

Raw sequencing data were processed with CASAVA 1.8.2 to generate FastQ files. Sequence reads were mapped onto mouse genome build mm9 using TopHat 2.1.0 (Trapnell et al., 2012). Gene expression values (FPKM; fragments per kilobase exon per million mapped reads) were calculated with Cufflinks 2.2.1 (Trapnell et al., 2012). Statistical analysis of differentially expressed genes (DEG) were performed with Partek Genomics Suite 6.6 using p value < 0.01 and absolute FPKM > 10 in at least 1 condition as criteria; differentially induced genes were further divided into two categories: fold change > 5 for highly-induced genes (HIGs); and > 2 and < 5 for weakly-induced genes (WIGs). The fold changes of gene expression were ranked and plotted using custom R code in Rstudio.

ChIP-Seq analysis

Sequencing data from ChIP-Seq were mapped onto mouse genome build mm9 using Bowtie 0.12.8. All ChIP-Seq experiments (p300, STAT4, STAT5, T-bet, H3K4me1, H3K4me3, H3K27Ac and H3K27me3) for both resting and activated NK cells isolated from wild-type mice were biologically duplicated. p300 ChIP-Seq for stimulated NK cells isolated from *Stat4*$^{-/-}$ mice was exceptionally done once, pooling from 25 mice. BigWig tracks were generated by the Hypergeometric Optimization of Motif EnRichment

program (HOMER) and visualized by Igv. MACS (version 1.4.2) was used for peak calling of transcription factor ChIP-Seq (p300, STAT4, STAT5 and T-bet) using a P value threshold of 1×10^{-5}. Published STAT5 ChIP-Seq data from *ex vivo* NK cells (Villarino et al., 2017b) were included in the final analysis. Downstream analyses and graph generation were performed with HOMER and R.

High-density p300 enhancer analysis

High-density p300 enhancers in resting and activated NK cells were called from p300 ChIP-Seq data using the findPeaks module with style as "super." Condition-specific high-density p300 enhancers and their nearby genes were further analyzed using the mergePeaks and annotatePeaks module, respectively, in HOMER. Statistical analysis and graphing were performed using custom R code in Rstudio.

ATAC-Seq analysis

Raw sequencing data were processed with CASAVA 1.8.2 to generate FastQ files. ATAC-Seq reads from two biological replicates for each sample were mapped to the mouse genome (mm9 assembly) using Bowtie 0.12.8. In all cases, redundant reads were removed using FastUniq (Xu et al., 2012). BigWig tracks were generated by HOMER and visualized by Igv. Only one mapped read to each unique region of the genome that was less than 175 base pairs was kept and used in peak calling. Regions of open chromatin were identified by MACS (version 1.4.2) (Zhang et al., 2008) using a P value threshold of 1×10^{-5}. Only regions called in both replicates were used in downstream analysis. Peak intensities ('tags' column) were normalized as tags-per-10-million reads (RP10M) in the original library. Downstream analyses and heatmap generation were performed with R using Rstudio.

Classification of enhancers with dynamic chromatin accessibility and activity

Genomic regions with dynamic enhancer activities upon NK activation were determined by merging reproducible p300 peaks from resting and activated NK cells using the mergePeaks module in HOMER. Chromatin accessibility of induced and extinguished p300 sites were further examined by analyzing their overlapping with reproducible ATAC-seq peaks in resting and activated NK cells. Only the dominant types (> 10%) of enhancer clusters (classes 1-6) were selected for motif analysis.

scRNA-Seq analysis

Sequence reads from all samples were processed and aggregated using Cell Ranger. Aggregated data was further analyzed by Seurat (Macosko et al., 2015). We visualized single cell gene-expression as tSNE overlays. We used the clustering produced by Seurat for the transcription module analysis. Downstream analyses and heatmap generation were performed with R using Rstudio. To explore cytokine-induced transcriptional modules in our scRNA-Seq data, we first defined modules by calling differentially expressed genes in our bulk samples, and then scored each single cell based on their expression of these genes. Specifically, we used PARTEK to identify differentially expressed genes (q-value < 0.05, |FC| > 2, at least 5 FPKM in one sample) in bulk samples treated with IL-2 and IL-12 for 6 hours compared to no stimulation. Next, we row-normalized the single cell gene expression matrix produced by Seurat to obtain Z-scores. To calculate a module score for each single cell, we added the Z-scores of upregulated genes and subtracted those of downregulated genes, then normalized by the total number of module genes.

Transcription factor motif analysis

Relative motif frequencies among distinct classes of enhancers were analyzed by the findMotifsGenome module in HOMER and custom R code in Rstudio.

Statistical analysis

Statistical significance of differential gene expression was assessed with non-paired two-tailed Student's t test. Statistical significance of association between two conditions was determined by using Fisher's exact test. Further information related to the statistical analyses performed is provided in the figure legends.